Neural Circuits Underlying Circadian Photoreception

Alexandra Neitz

A dissertation

submitted in partial fulfillment of the

requirements for the degree of

Doctor of Philosophy

University of Washington

2023

Reading Committee:

Horacio de la Iglesia, Chair

Jennifer Stone

Ethan Buhr

Program Authorized to Offer Degree:

Molecular and Cellular Biology

University of Washington

Abstract

Neural Circuits Underlying Circadian Photoreception

Alexandra Neitz

Chair of the Supervisory Committee:
Horacio de la Iglesia
Department of Biology

Light is an important environmental signal that affects many different aspects of physiology and behavior to allow organisms to both predict and respond to their surroundings. For example, light influences the timing of biological clocks or circadian rhythms. Although circadian rhythms are endogenous and persist in the absence of environmental cues, they can be reset or entrained by light and other environmental signals. In addition to circadian rhythms, other aspects of biology such as neuroendocrine function, mood, alertness, and cognition are also influenced by light. Therefore, the timing, duration, and quality of light plays an important role in maintaining physical and mental health. Although these light-driven circuits evolved in a natural light-dark cycle, electrical lighting and urbanization have reduced human light exposure during the day and increased light exposure at night. This pattern of light exposure has negatively impacted human health and performance. The goal of my thesis is to contribute to understanding these light-driven

circuits, which could be used to advise the use of light to mitigate negative effects of the modern light environment.

TABLE OF CONTENTS

LIST OF FIGURES

LIST OF TABLES

ACKNOWLEDGEMENTS

Thinking back to when I was first applying to graduate school, I remember my mom—who is a molecular biologist at the University of Washington—telling me that I should apply to the University of Washington Molecular and Cellular Biology (MCB) Program. After that, it was my dream to join the MCB program. Having been lucky enough to manifest that dream, I can say that it was all I imagined and more. First and foremost, my time in graduate school would have been impossible without the support of my family. I know many graduate students say this, but in my case it is even more true. Both my parents work in vision and I collaborated with them on several projects that I present here. In addition to supporting my experiments, they have also provided emotional support through the uncertainties of graduate school. I would also like to thank my husband Evan, who accompanied me to the lab on weekends or late at night when I had to check on an experiment and listened to my anxieties and hardships over the past 5 years.

I would like to thank my advisor, Horacio de la Iglesia, for providing me with the resources that made this work possible and providing the appropriate balance of mentorship and independence. Through this guidance, I was able to explore the best ways to collect and analyze my data. On multiple occasions, Horacio sent me to other universities to learn new techniques and these trips were invaluable to my development as a scientist and to the progression of my experiments. I would especially like to thank Mark Ellisman and Keunyoung Kim from the University of San Diego, who collaborate closely with us on the work presented below. Thank you for processing electron microscopy samples and providing support for the analysis of those samples.

My committee has provided me with valuable feedback on the work that I present in the following pages. They have always been willing to meet and discuss experiments outside of annual committee meetings and have always engaged in fruitful discussions that have improved the experiments that I present here.

For providing me funding for 1 year of my graduate dissertation, I would like to thank the University of Washington Vision Training Grant (VTG). Beyond the funding support, workshops given through the VTG has given me insight into how to apply for future jobs.

I have worked with three undergraduates who have supported me in completing these projects. I would especially like to thank Bryn Carter who has stuck by my side for more than 3 years and has stayed late to get data for timepoints countless times. I would like to thank Edward Young, who helped validate the machine learning algorithm used to obtain the bulk of the data in chapter 3. And thank you to David Dias, who helped process image files.

Thank you also to the staff scientists in the Vision Core Facility who helped prepare reagents and/or collect data presented here: Michelle Giarmarco, Jessica Rowlan, and Ed Parker.

One of the best parts of working in the de la Iglesia lab is that Horacio hires the best people, who also turn out to be the best scientists. I would especially like to thank Ivana Bussi, who was a post-doctoral scholar in the lab for my first 3 years of graduate school. She gives the best advice for experiments, careers, and life! Thanks to everyone who made the de la Iglesia lab a great place to work; Glorianna Gutierrez, Hannah Zaini, Alicia Rice, Leandro Casiraghi, Asad Beck, Dani Marinelli, and Victor Zhang.

Chapter 1. INTRODUCTION

1.1 THE RETINA

The retina is strikingly complex, yet neatly organized into distinct layers consisting of 5 classes of neurons, which are conserved across all vertebrate species. The five classes of neurons are classical photoreceptors (rods and cones), horizontal cells, bipolar cells, amacrine cells, and retinal ganglion cells (RGCs). Phototransduction is typically considered to start at the classical photoreceptors. The signal is then relayed through the retina, finally reaching the retinal ganglion cells (Figure 1.1). RGCs project to various brain regions controlling both image and non-image-forming functions. One subset of retinal ganglion cells contains a photopigment called melanopsin, which renders them intrinsically photosensitive (ipRGCs) and, as a consequence, they do not need to receive signals from classical photoreceptors to respond to light. The ipRGCs are the RGC subtype that transduces light signals to brain regions controlling several non-image-forming functions including circadian rhythms, mood, and cognition.[1] Melanopsin was first proposed to be an important photopigment for non-image forming functions[2] after the discovery that rods and cones are not necessary for photoentrainment in mice.[3] Later, it was shown that mice lacking melanopsin could still photoentrain, suggesting that either rods and cones or melanopsin are sufficient for photoentrainment.[4] However, the relative roles of rods and cones remained unclear. Recently, it was shown that mice that only have cone photoreceptors are able to photoentrain.[5] This suggests that melanopsin or cones are sufficient for photoentrainment. In contrast to cone circuits that are sensitive to color, melanopsin is sensitive to a broad spectrum of light and is best at detecting changes in illuminance.[6]

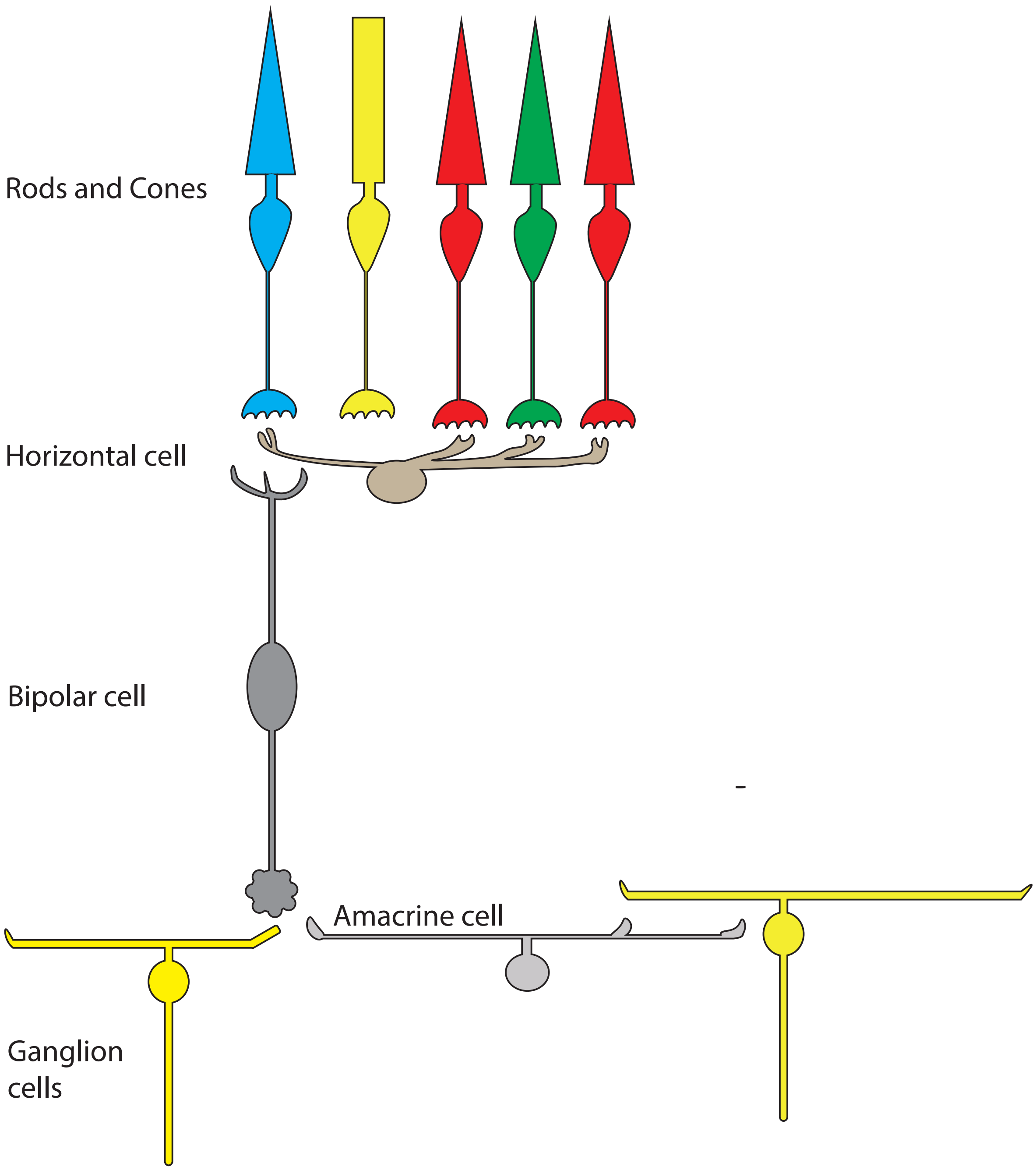

Figure 1.1 Retinal anatomy. Rods and cones are photosensitive cells that respond to light stimuli and send the information through the retina, ultimately reaching retinal ganglion cells, which project to the brain.

In nature, the environmental illuminance changes frequently and drastically across the day depending on weather, shade, and shelter. Furthermore, solar light changes color at dawn, and dusk and these changes in chromaticity may be a more reliable environmental signal for some non-image-forming functions, such as circadian entrainment, especially in cone-dominant species such as humans. Consistent with this, melanopsin-containing ipRGCs were also discovered in the primate retina and are strongly activated by rods and cones.[7] The first studies of ipRGCs did not distinguish between subtypes, but later anatomical studies revealed 2 subtypes that are functionally distinct. The M1 type ipRGCs have higher melanopsin expression and melanopsin light responses compared to the M2 type, which are more strongly driven by rod and cone responses.[8,9] In mice, the only RGCs that project to the suprachiasmatic nucleus (SCN) are a subset of M1 ipRGCs.[10] However, whether this is true in primates is not yet known. Aside from M1 and M2 subtypes, additional functional categories of ipRGC have been discovered, but how they relate to these two anatomical subtypes is unclear.[11]

Although ipRGCs receive input from both rods and cones, my focus is on the cones and more specifically, S-cone circuits, which are spectrally opponent such that they are sensitive to color. The S-cone opponent circuits are the best candidate for sensing chromaticity changes at dawn and dusk. Cone photoreceptors receive lateral inhibition from neighboring cones through horizontal cells, which creates center-surround receptive fields and color opponency in the retina. The cone photoreceptor responses, already subject to lateral inhibition, are then transmitted to bipolar cells, which relay the responses through the retina. S-cones receive lateral inhibition exclusively from HII horizontal cells, which gather information from surrounding S, M, and L cones. Thus, S-cone photoreceptor outputs are S vs (L+M) color opponent.[12] This opponency is relayed through the retina via parallel ON and OFF pathways. The S-ON pathway is activated by short and inhibited by long wavelength light and the S-OFF pathway is activated by long and inhibited by short wavelength light. Electrophysiology recordings showed that M1 ipRGCs display a rare S-OFF response, but mysteriously this S-OFF response was blocked by inhibiting S-ON bipolar cells.[7] This paradox was recently explained through serial block face electron microscopy, which demonstrated that the S-ON bipolar cell signal to M1 ipRGCs is inverted by an amacrine cell.[13] While reconstructing other RGCs receiving S-ON bipolar cell input, M2 ipRGCs were discovered to receive excitatory inputs from S-ON bipolar cells almost exclusively.[14] Therefore, two blue-yellow color opponent ipRGC pathways that have opposite spectral tuning have been reported.

Because the spectral sensitivity of melanopsin peaks at 483 nm, it was assumed for many years that the sensitivity of non-image-forming functions to short-wavelength light was due to melanopsin alone. Given the importance of these non-image-forming functions on mental and physical health, light therapies aimed to improve mood and align circadian rhythms with the natural light-dark cycle were designed to target melanopsin. Melanopsin is ~1000X less sensitive than cone opsins[6] and so these light therapies use high illuminance and require long durations to illicit the desired effects. In contrast, cone photoreceptors are the main contributor to circadian photoentrainment when the lights are low-illuminance and the duration of the light is short.[15] However, these studies did not consider the color-opponency of ipRGCs, and so the test lights were static and appeared either blue or green. Despite the lower illuminance and shorter durations required for successful outcomes, the apparent color of the lights can make them uncomfortable to use. We now know that there are three pathways through which ipRGCs can respond to short-wavelength light: melanopsin, the S-OFF M1 ipRGC pathway, and the S-ON M2 ipRGC pathway. Each of these pathways has distinct mechanisms that can be separately targeted with the right experimental design. In the second chapter, I test the relative contribution of melanopsin and the blue-yellow color opponent pathways in human circadian entrainment.

1.2 Circadian Rhythms and Light

Virtually all organisms anticipate daily changes in the environment using an internal biological clock that coordinates the timing of physiology and behavior. Circadian rhythms are the outputs of the clock, such as 24-hour rhythms in metabolism, hormone release, and activity-rest cycles. These circadian rhythms are endogenous and continue to occur rhythmically in constant conditions (i.e. the absence of environmental time signals). However, in constant conditions, the period is close to, but not equal to 24-hours. In humans, the average endogenous period is slightly longer than 24-hours.[16] Therefore, to match the 24-hour periodicity of the environment, an important property of circadian rhythms is that they are reset, or entrained to, environmental signals. Environmental signals with 24-hour periodicity that can reset the clock are called zeitgebers, which is German for "time giver". The strongest zeitgeber is the light-dark cycle. Light can acutely change the phase of the circadian clock. The direction and magnitude of the circadian phase resetting is dependent on the time of day (or phase) of the biological clock at which light stimulates it; this relationship is described by the phase response curve (PRC, Figure 1.2). Light during the clock's "subjective" morning resets the clock to an earlier time, and this is called a phase advance. In contrast, during the subjective evening, light causes a phase delay, moving the clock to a later time. Light in the middle of the day has little effect on the clock. When exposed to a natural light-dark cycle, the light-induced phase advance is offset by a phase delay in the evening, leading to a net shift that will keep the clock in synchrony with the external light-dark (LD) cycle. Due to electrical lighting and urbanization, the modern light environment differs drastically from that of the natural light cycle. People receive less light in the morning, less exposure to daylight during the day and more light in the evening after sunset. This light exposure disproportionally stimulates the phase delay region of the PRC, and so overall people's internal biological clocks tend to be delayed relative to solar time.[17-19]

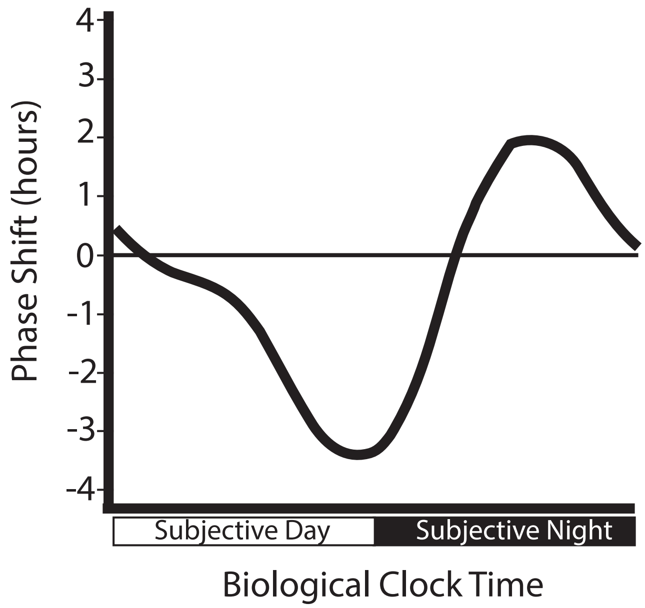

Figure 1.2 Human phase response curve to a 6.7 hour pulse of bright white light.[20]

There is a spectrum of internal clock phases, with some people having more delayed rhythms than others. The preference for staying up late or going to bed early is referred to as chronotype and is driven by the timing of the internal clock.[21] Since the circadian clock in part controls sleep and wake cycles, a delayed clock delays sleep onset until later in the evening. However, work and school schedules are set to solar time, such that noon is set to the time at which the sun reaches its daily peak. Therefore, during the week many people must wake up early, before the end of their biological night, cutting off much-needed sleep. Due to the sleep debt accumulated on the weekdays, many people, especially adolescents, undergo sleep recovery in which they sleep later and longer on the weekends, which can delay the clock.[21-23] This creates a cycle in which the clock is delayed on weekends, making it difficult to go to bed early on Sunday nights and cutting off sleep when waking up for work or school on Mondays. Throughout weekdays, the clock shifts to an earlier phase, but it still does not completely align to solar time.[18] In fact, even on weekdays the internal clock is on average more than 2 hours delayed relative to solar time.[18] By the weekend, sleep debt has accumulated from the clock being delayed, and sleep recovery delays the clock even more.

The difference in sleep timing on weekdays compared to weekends is called social jetlag and is associated with worse health outcomes such as depression and metabolic disease.[21] This is especially of concern in people with later chronotypes. One way to ameliorate this problem is to shift circadian phase to align with solar time throughout the entire week and weekends. This would allow people to get sufficient sleep on weekdays and eliminate the need for sleep recovery on weekends. This has been achieved in experiments in which human subjects camp outdoors.[18,19] Under these conditions, people are exposed to natural light (and only natural light) for the entire day, which resets the clock such that circadian phase is perfectly aligned to the natural light-dark cycle. Importantly, differences in chronotype were diminished when people were camping.[19] In other words, under strong enough zeitgebers, all chronotypes can align to solar time. However, receiving enough solar light while maintaining a modern lifestyle remains a challenge. For this reason, many people have turned to indoor light therapies. The protocol for light therapies is to use them in the morning to increase light exposure in the phase advance portion of the PRC. Many current light therapies target melanopsin. One study testing circadian phase shifts to either 1h or 6.7h of bright white light (targeting melanopsin stimulation), showed that while human circadian phase advances to 1h pulses of bright white light occur, the responses are much more robust to the longer duration light.[20] Therefore, it is uncertain if the 1h bright white light is a strong enough zeitgeber for later chronotypes. More recently there has been interest in light therapies with different spectral properties, with the goal of stimulating cone photoreceptors. For example, one study concluded that cones play a role in phase resetting by using monochromatic lights of different wavelengths.[24] However, this study did not take into consideration the color opponency of the cones and was unable to make conclusions about the relative contribution of the cones versus melanopsin. Additionally, since cones have transient responses, the cones may not have continued to respond over the duration of the light pulse. Another study aimed to stimulate the cones' transient responses by giving consecutive millisecond flashes of dim (~500 lux) white light in the evening and found that on average it causes 45 min phase delay.[25] However, it is unlikely that people would be willing to use a flashing light therapy because of how uncomfortable it is to use. In fact, none of the current light therapies are comfortable solutions, either because they are too bright or composed of colors that are hard to adapt to, and therefore likely have low compliance for the patients using them. To design a better light, we need a deeper understanding of the circuits that drive circadian photoentrainment.

In the second chapter of my thesis, I hypothesize, based on retinal ultrastructural anatomy, that the blue-yellow color opponent circuits are strong drivers of circadian photoentrainment. Theoretically, a dim nominally white light (that is comfortable to use) could be made that achieves strong blue-yellow opponent responses. This light would alternate between the S-ON and S-OFF response by alternating between 427 nm light and 545 nm light. The light would flash between the two wavelengths at a speed that would not be perceived by conscious color vision and therefore would appear static. Furthermore 638 nm light could be added to make the light appear nominally white. In the second chapter of my thesis, we make progress toward validating such a light. The light that we use still appears to flicker, but it is nominally white. With future prototypes, a light that does not flicker at all can be achieved. This has the potential to be a very strong photic zeitgeber capable of advancing later chronotypes that is also comfortable to use.

1.3 The SCN

In mammals, circadian rhythms in behavior and physiology are orchestrated by the suprachiasmatic nucleus (SCN) of the hypothalamus. The SCN is a paired structure located on either side of the third ventricle above the optic chiasm. The SCN is classically split into core and shell subregions, which are defined by the differential expression of neuropeptides.[26] Neurons expressing arginine vasopressin (AVP) are located in the shell, and neurons expressing vasoactive intestinal polypeptide (VIP) are located in the core (Figure 1.3). Classically, it was thought that the core receives retinal input and relays that information to the shell, and the shell then projects to regions outside of the SCN to coordinate circadian rhythms across the body. However, these functions in the mouse are more shared between the shell and core than originally thought. For example, retinal projections in the mouse innervate the entire SCN,[27] not just the core, and VIP neurons of the core project outside the SCN and control some output rhythms such as the rhythm in corticosterone[28] and the timing of the daily siesta[29]. Furthermore, although neurotransmitter expression has been a convenient categorization of neurons within the SCN, gene expression (RNA-seq)[30], structural[31], and functional studies[32] have demonstrated that it may be important to consider additional subdivisions to elucidate how the SCN functions as the central mammalian pacemaker.

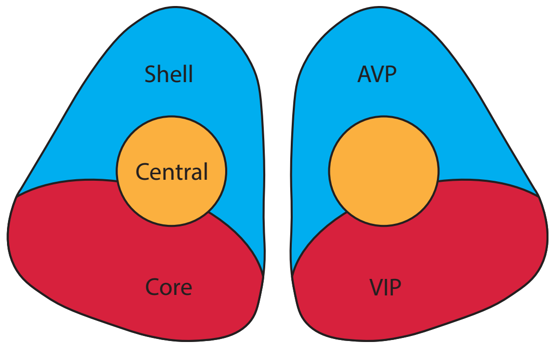

Figure 1.3 Subregions of the SCN. The SCN is split into 3 subregions based on expression of neuropeptides. The shell contains predominantly AVP expressing neurons, while the core consists of neurons that express VIP.

1.3.1 *Synchronization*

SCN neurons and glia, like virtually all cells in the body, contain a molecular clock consisting of a transcriptional translational feedback loop (TTFL) that oscillates autonomously. Although there are several interlocked loops, the core loop consists of the transcriptional activators CLOCK and BMAL, which bind to the promoters of families of *Per* and *Cry* genes to activate them. Following the dimerization of PER and CRY proteins in the cytoplasm, the complex enters the nucleus and sequesters CLOCK and BMAL, inhibiting further transcription of *Per* and *Cry* genes. Genes within the molecular clock contain cAMP/calcium response elements (CREs), which makes the TTFL sensitive to neuronal activation. This is critical because signaling among SCN cells allows the cells to be synchronized to one another, and this synchrony makes the SCN a uniquely robust oscillator. One piece of evidence for this is that while SCN explants can sustain oscillations for several months, fibroblasts in ex vivo cultures have damped oscillations.[33] This damping of population-level oscillations is due to a loss of synchrony among fibroblasts, which is prevented in the SCN through specific network properties. Additionally, the intercellular coupling of SCN neurons allows the SCN to maintain oscillations in molecular clock mutants, which represents an emergent property of the SCN tissue clock.[34]

One source of this intercellular coupling is synapses. Blocking classical neurotransmission in *ex vivo* SCN slices with tetrodotoxin (TTX) causes individual neurons to become desynchronized and damps individual and population-level amplitude.[35] While this demonstrates that overall synapses are critical to SCN timekeeping, the question remained whether the specific organization of the synapses was important. To answer this, the molecular clock of individual neurons was measured from dissociated neurons *in vitro*. Although many of the individual molecular clocks remained rhythmic, the neurons were not synchronized to one another, contributing to a damped population-level oscillation.[34] Therefore, the specific synaptic connections that neurons make with one another are a critical property of the SCN network.

Virtually all SCN neurons are GABAergic. Despite its abundance in the SCN, the role of GABA in SCN timekeeping remains unclear. Application of GABA can synchronize SCN neurons,[36] but GABA is not necessary for SCN synchrony. In fact, blocking GABA signaling can increase the amplitude of the firing rate rhythm.[37] Interestingly, it was later shown that GABA acting through $GABA_A$ receptors can either promote or inhibit synchrony depending on the coupling state of the SCN.[38] In other words, if all SCN neurons are in phase with one another, GABA acts as a desynchronizer. On the other hand, SCN neurons in different regions of the SCN can be in antiphase under longer photoperiods (e.g. 16-hours light:8-hours dark, 16:8LD), and under these conditions GABA acts as a synchronizer. One possibility is that GABA has distinct functions in different populations of SCN neurons. Consistent with this, deleting the vesicular transporter for GABA (*Vgat*) in only VIP or only AVP neurons has differential effects on entrainment and free-running rhythms.[39,40] However, the animals do not become arrhythmic in either case.

In addition to communicating through classical synapses, SCN neurons also differentially express and release neuropeptides, as introduced above. These neuropeptides have a hierarchy, with VIP being the most important for the synchronization of SCN neurons.[41] Mice lacking either VIP or its receptor VPAC2 display abnormal circadian behavioral phenotypes,[42,43] and this is likely due to desynchronization among SCN neurons, which was demonstrated in SCN explants of VIP (*Vip*$^{-/-}$) or VPAC2 (*Vipr2*$^{-/-}$) knockout mice.[44,45] The rhythm amplitude of the slices is restored with the application of VIP in *Vip*$^{-/-}$ slices, but not *Vipr2*$^{-/-}$ slices.[46] In contrast, the addition of a wild-type graft can restore the rhythm amplitude in *Vip*$^{-/-}$ slices and to a lesser extent in *Vipr2*$^{-/-}$ slices. The presence of the neuropeptides AVP and gastrin-releasing peptide (GRP) account for some of this rhythm restoration because when antagonists of these neuropeptides are added, the rhythm cannot be fully restored.[41] Furthermore, the AVP antagonist has a larger effect on inhibiting the restoration than the GRP antagonist. Although AVP is weak synchronizer compared to VIP, its most important role within the SCN may be to confer resistance to external perturbation. Mice lacking AVP receptors V1a and V1b shift immediately under jet lag conditions, whereas wild-type mice display transients (i.e. behavioral circadian rhythms shift a little day by day).[47]

1.3.2 *Entrainment*

SCN neurons can entrain to the light-dark cycle through ipRGC-to-SCN signaling. Light information is passed from the ipRGCs to the SCN via the release of glutamate, which binds to NMDA and AMPA receptors. This leads to calcium influx and ultimately to the activation of cAMP/calcium response element binding (CREB) proteins, which can adjust molecular clock time to synchronize with the light-dark cycle.[48]

First studies of retinal innervation to the SCN were performed in rats and showed that retinal projections reach only the ventral SCN.[26] However, in mice, the entire SCN is densely innervated by ipRGCs such that VIP, AVP, and GRP neurons all receive retinal input.[27] Despite this dense retinal innervation, current evidence suggests that ventral neurons such as the VIP neurons are most important for entrainment. First, the dorsal SCN requires more stimulation than the ventral SCN to respond to light.[27] Second, inhibiting VIP neuron activation with chemogenetics during a light pulse attenuates phase shifts.[49] Finally, electron microscopy studies revealed that a subset of SCN neurons form an interconnected network of dendrodendritic synapses.[31] This network is hypothesized to be tightly coupled via inhibitory GABAergic synapses. The ipRGCs preferentially innervate neurons within this network. This result is consistent with the hypothesis that there is a small network of ventral SCN neurons that are the first to entrain to the light-dark cycle, and those neurons then send signals to entrain the rest of the SCN.[50]

1.3.3 *Plasticity*

It is quite incredible that the circadian system is both robust against external perturbations, and also sensitive to the *appropriate* environmental signals. One example is the ability of the clock to shift to light in a phase-dependent manner. In other words, the ability to shift in response to light is gated by circadian time. This gating is in part explained by time-dependent differences in the sensitivity of the SCN to glutamate. Early studies in rats showed that NMDA receptors are more active in the night when the circadian system shifts in response to light.[51] This result is consistent with studies that found SCN neuron calcium transients change more in response to NMDA during the night compared to the day.[52] Although these early studies in rats did not differentiate among SCN cell types, it is likely that the neurons postsynaptic to these retinal inputs were VIP neurons. This prediction is consistent with evidence in mice that showed VIP neurons have high spontaneous calcium activity during the day and that any additional stimulation with NMDA cannot raise neuron activity. However, during the night spontaneous calcium is low in VIP neurons, and NMDA application increases this activity.[49]

Interestingly, in rats, VIP neurons had increased innervation by glutamaterigic fibers during the day compared to night, and this was due to relocalization of synapses, as opposed to increased active zones on established appositions.[53] This result is consistent with studies showing components of vesicle trafficking are circadian-regulated in mice.[54] In addition to neuron structural changes, glia also undergo daily structural rearrangements in rats. In the ventral SCN, VIP neurons are covered by glia more during the night than the day.[55] This rhythm is in antiphase with the rhythm of glutamatergic synapses to VIP neurons. Together, these findings suggest that glial cells come between pre-synapses and the post-synaptic membrane of VIP neurons during the night, while during the day glia retract, allowing synapses to reform.

Overall, the function of these daily structural changes remains unclear, but they may be important for mediating the sensitivity of VIP neurons to light. The evidence so far suggests that plastic functional connections, in which daily changes in retinal axons are coupled with circadian control of the VIP neuron post-synaptic response to glutamate, are an essential property of the SCN network. This functional plasticity could provide a mechanism by which the circadian system is able to adapt to the appropriate environmental stimuli, while remaining robust against the wrong stimuli. In the third chapter of my thesis, I further explore the circadian and daily structural plasticity of the VIP neurons.

Chapter 2. TOWARD AN INDOOR LIGHTING SOLUTION FOR SOCIAL JET LAG

2.1 INTRODUCTION

People who spend most of their time under artificial light often suffer a phase delayed circadian rhythm.[17-19] The discrepancy between an individual's delayed biological rhythm and the daily timing determined by social constraints like school and work schedules causes "social jet lag"[21] which is associated with disturbed sleep, daytime fatigue, reduced cognitive function, and a general feeling of unwellness. A potential solution to social jet lag is to develop artificial lighting that is capable of stimulating ipRGCs in the morning during times when such stimuli produce phase advances (Figure 2.1 A).[56] Regarding circadian rhythms, there has been an emphasis on the effects of light on the intrinsic photopigment, melanopsin, however, ipRGCs can be activated by light absorption by cone photoreceptors whose signals are carried by color opponent circuitry (Figure 2.1 B) in which short (S) and long (L) plus middle (M) wavelength cones have opposite signs.[8,13,14] The color opponent input to ipRGCs may have evolved so that changes in the color of sky at dawn and dusk (Figure 2.1C) can contribute to synchronization of the internal circadian clock such that the internal biological night begins at sunset and ends before wake time, just after sunrise. Previous experiments have provided evidence for a role for color opponency in circadian phototransduction[57] and clear evidence for an S-cone contribution in humans.[24,58]

Compared to melanopsin, cone-opponent circuits activate ipRGCs at much lower thresholds.[7] Thus, at common indoor low illumination levels, lights optimized to stimulate the color-opponent circuits could be much more effective in producing circadian phase advances than typical white artificial lighting. Color opponent circuitry in humans is normalized through experience to null to white.[59] Thus, even though artificial white light stimulates S-cones, because the excitatory and inhibitory cone components of the S vs. (L+M) circuitry are balanced by white light, it is predicted to have little net effect (Figure 2.1D, bottom left). Narrowband lights that primarily stimulate one side of the opponent circuit are predicted to be much more effective (Figure 2.1D, bottom middle). Finally, the circuity carrying cone signals has relatively transient response properties, so under laboratory conditions using narrow band lights that primarily stimulate S-cones, their contributions decay upon extended light exposure.[24,58] Thus, the intensity, spectral and temporal characteristics of the light must all be considered when developing indoor illumination capable of combating social jet lag.

We designed a light that stimulates color-opponent inputs to ipRGCs by temporally alternating short and longer wavelength components that strongly modulate short-wavelength sensitive (S) cones. We determined the ability of a morning exposure of this light to produce a phase advance capable of combatting social jet lag compared to a static white light and a static narrow band blue light. Our goal is to evaluate the most effective dynamic lighting approach for circadian photoentrainment at the comparatively low general lighting lux levels typical for homes, offices, schools, and health care facilities. We hypothesize that practical lighting solutions that drive cone-based color-opponent inputs to ipRGCs in the early morning can mediate circadian phase advances that will promote improved mood and cognitive function, combat social jet lag and other circadian problems such as seasonal affective disorder.

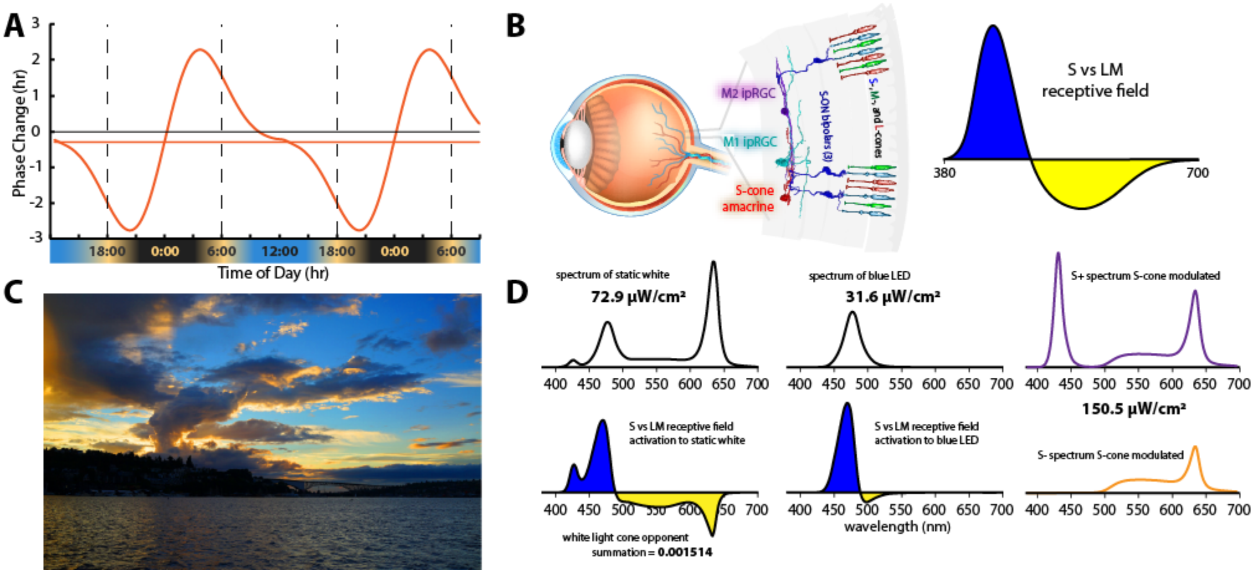

Figure 2.1 **(A)** Phase response curve[56] aligned with earth time so that the beginning of the internal biological night occurs at sunset and the end of the internal biological night occurs before wake time just after sunrise as indicated below the x-axis of the curve. **(B)** (left) Illustration of the color vision circuitry for S-ON and S-OFF types of primate ipRGCs. (right) Illustration of the spectrally opponent response of an S-ON ipRGC with S - (L+M) cone inputs. **(C)** Image of sunset in Seattle Washington illustrating how contrasting short and long wavelength light near the horizon produces a stimulus capable of driving spectrally opponent inputs to ipRGCs making them act as sunrise/sunset detectors. **(D)** Spectral distributions of experimental light stimuli and their predicted effects on the color opponent inputs to ipRGCs. (Top left) Spectrum of the experimental white light with chromaticity coordinates 0.333, 0.333. (Top middle) Spectrum of the LED-derived experimental "blue" light with a spectral peak at 476 nm. (Bottom; left and middle) the product of wavelength-by-wavelength multiplication of the spectral distribution of the white light (Bottom left) times the spectrally opponent response of an ipRGC. Integration of the curve across wavelength yields the predicted very small relative response of the ipRGC to the white light. (Bottom middle) The product of multiplication of the spectral distribution of the blue light times the spectrally opponent response of an ipRGC. Integration across wavelengths yields the predicted large relative response of the ipRGC to the blue light. (Right) The two spectra which are alternated to produce the S-cone modulating light.

2.2 METHODS

All methods were performed in accordance with the relevant guidelines and regulations. Data collected and used in this study are available upon request.

2.2.1 *Minature, programmable, and portable ganzfeld design*

Modified safety goggles were fitted with diffusers and LED illumination to provide light stimuli (Figure 2.2A). LEDs and LED driver circuitry were mounted to curved plastic-corrugated aluminum bands which were, in turn, mounted to the googles by metal standoffs. A spectrally flat transmissive diffuser (Lee filters, LEELux #400RW) replaced the original lens of the goggles. Three sets of four high powered LEDs (Luxeon CZ line by Lumileds) were mounted in each goggle stimulator, L1CU-VLT1 with peak at 426 nm, L1CU-BLU1 with peak at 476 nm, L1CU-LME1 with peak at 539 nm, and L1CU-RED1 with peak at 634 nm. LEDs had a continuous forward DC current rating of 350 mA, but driver circuitry was designed to underdrive them at 100 mA per channel. Three aluminum circuit boards with the four LEDs were positioned at regular intervals across the curved aluminum band with the middle pad positioned at the center of the goggle. This arrangement provided diffuse homogenous full-field illumination (for example, Figure 2.2B, blue (left) and static white (right)) covering approximately 130 degrees of visual angle.

The goggles' illumination was controlled by custom made electronic constant current Pulse Width Modulation (PWM) control driver circuitry. This device was configured to allow LED settings to be stored on an EEPROM. These devices were calibrated and programmed in the laboratory and sent home with individual subjects. The spectral characteristics of the light reaching the eyes were measured using an CS-2000A spectroradiometer (Konica Minolta) positioned one meter behind each goggle. The two spectrums that were alternated temporally to drive high S-cone modulation were calculated theoretically using retinal sensitivities for S-cone, melanopsin, M-cone, and L-cone retinal sensitivities given by a photopigment template [60] with peaks set at 419 nm, 480 nm, 530 nm, and 559 nm, respectively, corrected for absorption by a 30-year-old lens [61]. For the S-cone modulating light, the ratio of S-cone activation between the temporally alternated spectrums was 100:1, while L- and M-cone activations were held constant between the two temporal phases. The alternating spectrums (Figure 2.1D right; top and bottom) were programmed onto the goggles and modulated at 19 Hz presented as a square wave with 50% duty cycle. The radiance of this dynamic white light measured at the back of the goggles was 150.5 $\mu W/cm^2$. The alternation of the two spectrums produced approximately 500 lux at the subject's pupil plane as measured with a lux meter (Digital Light Meter, LX 1330B). Melanopsin activation was determined by integrating the measured time-averaged spectrum with the corneal sensitivity for melanopsin. The two other conditions, the static white light spectrum (Figure 2.1D, top left) which produces a radiance measured at the back of the goggles of 72.9 $\mu W/cm^2$ and the static blue spectrum from the 476 nm LED (Figure 2.1D, top middle) which produces a radiance measured at the back of the goggles of 31.6 $\mu W/cm^2$, were adjusted in intensity to produce the same time-averaged melanopsin activation as the S-cone modulated light. Thus, all three experimental light conditions were equated for time-averaged melanopsin effectiveness.

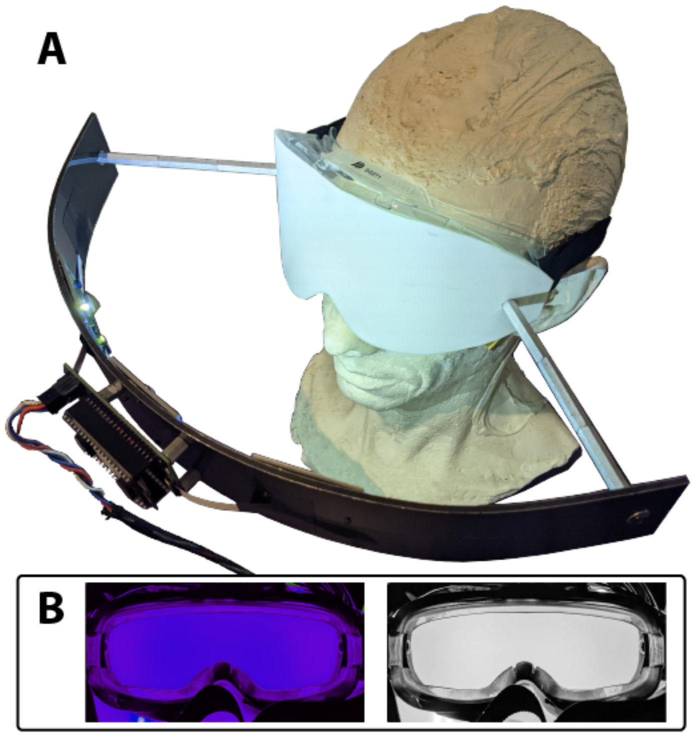

Figure 2.2 **(A)** Battery powered portable "ganzfeld" light stimulator with self-contained uniform four color LED illumination programmable in intensity, temporal and spectral characteristics. **(B)** The front diffuser of the illumination system goggles uniformly illuminated by the 476 nm LEDs (left) and static white (right).

2.2.2 *Human subjects*

The Institutional Review Board at the University of Washington approved the human subject's research. Research involving human subjects was performed in accordance with local and federal regulations. Human subjects research adhered to the principles embodied in the Declaration of Helsinki. Informed consent was obtained from all participants. The subjects were adult volunteers from the University of Washington community in Seattle.

Ten subjects were recruited, and six healthy adult (2 male and 4 female) subjects (mean age = 30; range 23-43) met inclusion criteria defined by having a robust rise in dim light melatonin onset between ca. 6:00 PM and 2:00 AM from saliva as measured by ELISA. Melatonin deficiency can have a variety of causes[62] including insufficient exposure to outdoor light as experienced by academics at high latitudes such as Seattle in winter time. Four subjects had little or no measurable rise in evening salivary melatonin levels and were discontinued after an initial baseline measurement. The six subjects continued with their daily academic lives during the winter months (December - February) in Seattle, WA over the course of the experiments. The purpose of the experiments was to determine the effects on circadian phase of three different lighting paradigms which were viewed for two hours centered 10.5 hours after individual subjects reached 20% of their Dim Light Melatonin Onset ($DLMO_{20\%}$). Lights administered at this time should produce the maximum circadian phase advance (Figure 2.1A). Circadian phase was determined from the rise in evening melatonin levels assayed from saliva samples. To measure phase accurately, it was important to identify subjects with a robust, reliable evening rise in salivary melatonin. In addition, it is important that our participants are stably entrained to the 24-hour environmental cycle even though we expect most members of the University of Washington community to suffer from some amount of phase delay. New recruits collected baseline evening salivary melatonin samples every hour from 5-6 PM until 12-2 PM. During this period, they were instructed to generally keep illumination levels as measured by an illuminometer below 10 lux. Short periods of higher illumination were allowed, when necessary, but were always kept below 30 lux. Subjects also confirmed that they were keeping a regular sleep-wake schedule in the days surrounding the experiment.

Of the six subjects who met the inclusion criteria, all were involved in studies related to circadian rhythms. As such, they were all very motivated to adhere to the grueling demands of the protocol. These included adhering to the strict dim evening lighting regimen, collecting saliva on a strict schedule, proper handling of the saliva samples and viewing the lights at the times and for the durations specified. We believe that having motivated and compliant, participants was key to obtaining precise and reliable results. However, this means that the highly ethical participants were not blind to the conditions or hypotheses. Salivary melatonin measurements are objective, so the fact that participants were not naïve could not bias the results. In addition, we took extensive measures to ensure the subjects' knowledge could not bias the results. The subjects received a box of tubes prelabeled with times in which they were to provide samples, two tubes for each hour. The subjects used timers to keep them on the precise schedule of taking samples each hour and storing them on dry ice. All the samples from a given evening were collected and processed according to the Salimetrics protocol, and the resulting the 96-well plate was read by an automated colorimeter system. An automated procedure was used to fit an integrated Gaussian (error function) by minimizing the sum of least squares. The goggles were pre-programmed for each lighting condition such that subjects did not have control of the spectral or temporal properties of the light or its intensity. The subjects followed a strict protocol dictating when and for how long to view each light condition. Phase advances in circadian phase are notoriously difficult to produce, so there is no way a subject's knowledge of a particular light condition could be responsible for the large phase advances observed in these studies.

2.2.3 *Experimental protocol for viewing light stimuli*

The experiment was conducted during the COVID19 pandemic. Safety protocols prevented participants from coming to the laboratory for experimental procedures: thus, all experiment procedures were conducted in participants' homes. Saliva samples were collected by the subjects at one-hour intervals starting 5-6 PM PST and placed on dry ice immediately after collection. Two separate saliva samples were collected at each time point, which were analyzed separately and averaged to minimize noise for each individual timepoint. Since the experiments were done in the winter in Seattle, saliva collection was done after sunset so there was no possibility of exposure to sunlight during saliva collection, and subjects stayed in their homes with the illumination generally kept below 10 lux and always below 30 lux. Circadian timing was measured by the dim light salivary melatonin onset (DLMO, Salimetrics melatonin ELISA). $DLMO_{20\%}$ was calculated as the time point at which melatonin levels reached 20% of the fitted peak-to-trough amplitude of each person's data. The data were fitted to an integrated Gaussian (error function) by minimizing the sum of least squares. Maximum phase advances were assumed to occur 10.5 hours after $DLMO_{20\%}$. Administrations of a 2-hour light pulse of the therapeutic lights were therefore centered around 10.5 hours after $DLMO_{20\%}$. Saliva was collected in the evening and melatonin levels were assayed using the Salimetrics kit the following day and subjects were informed of what time to administer the light the next morning. Lights were administered in the subjects' homes the morning after the baseline internal circadian timing was measured. To be clear, subjects viewed the light conditions 35.5 hours after their baseline $DLMO_{20}$. To determine the phase advance caused by each light, circadian timing was remeasured by collecting saliva samples the evening of the day the light was administered. Phase advances were calculated as the difference between $DLMO_{20\%}$ after light administration and baseline $DLMO_{20\%}$. Differences in phase produced by the light treatments were evaluated using a paired t-test using each person DLMO measurement before and after treatment as a pair.

2.3 RESULTS

2.3.1 *Participants' circadian phase relative to solar time*

When humans are exposed only to natural light, the internal circadian clock synchronizes to solar time such that the internal biological night begins at sunset and ends before wake time just after sunrise [19] (Figure 2.1A). We used dim light salivary melatonin onset (DLMO) as a measure of circadian phase. Figure 2.3A shows the rise in evening melatonin levels assayed from saliva samples for the six subjects who participated in this study (each subject is represented by a different color). Compared to being synchronized to solar time (shown by the dashed gray curve; Figure 3A), we found that, on average, subjects were phase delayed by 2.8 hours. Baseline results for each subject were comparable across multiple days, indicating that while all subjects were phase delayed, they were still entrained to the 24-hour environmental cycle. These phase delay results are like those observed earlier for young academics[19], highlighting the need for an artificial lighting solution that can effectively bring the sunlight indoors. Later chronotypes are associated with longer phase delays[19] consistent with the considerable variability in the phase delays among the six subjects.

2.3.2 *Spectral and temporal properties of lights capable of producing phase advances*

We measured the effectiveness of lights with different spectral and temporal properties in generating circadian phase advances. Three light conditions were calibrated to produce the same time-averaged effect on melanopsin, but to have large differences in their effect on the recently discovered color vision circuits that drive M1 and M2 ipRGCs[13,14], as illustrated in Figure 2.1B. One light had the same CIE coordinates (x = y = 0.33) as an equal energy white and produced an illuminance of 500 lux (Figure 1D, top left). A second light was blue, derived from an LED (476 nm peak) (Figure 2.1D, top middle). These two lights are predicted to have very different effects on the color vision circuits carrying chromatically opponent signals from short (S-), middle (M-), and long (L-) wavelength sensitive cones that drive ipRGCs in primates[13,14] (Figure 2.1D, bottom middle and left). Primate ipRGCs display an S vs. (L+M) color-opponent spectral response (Figure 2.1B, right). The white light drives both the excitatory and inhibitory sides of the color-opponent response, thus producing almost no net drive to the ipRGCs from cones. In contrast, almost all wavelengths in the blue light stimulate the S-cones on the "blue" side of the response of the color-opponent system. Thus, the white light is expected to produce a null response, and the blue light is predicted to be many times more effective at driving the color-opponent pathways upstream of the ipRGCs (Figure 2.1B, left and middle).

To evaluate the ability of lights with different spectral and temporal characteristics to advance circadian phase, we followed a 3-day protocol for each light condition. On the evening of the first day, subjects collected saliva samples every hour starting at 5-6 PM ending at 12-2 AM. The following day, the samples were analyzed to measure the rise in melatonin the evening before and the time of DLMO was determined for each subject, defined as the time the melatonin levels reached 20% of maximum.[63] On the morning of the third day of the protocol, each subject viewed a test light for two hours centered 10.5 hours after their individual DLMO. This corresponds to the time of circadian cycle expected to produce the maximum light-induced phase advance (Figure 2.1A).[56] On the evening of the same day, subjects again collected saliva samples that were used to evaluate whether the light exposure produced a phase advance.

Figure 2.3B shows the results for the static white light. After exposure to the static white light, the average rise in evening salivary melatonin levels did not differ significantly from the baseline, measured before exposure). The slight phase delay after the exposure is within experimental error ($p<0.05$; paired t-test).

In contrast to the results for the static white light, Figure 2.3C shows the phase advance produced by the 476 nm blue light that was equated in melanopsin effectiveness to the white. The blue light produced a phase advance of 40 minutes (Figure 2.3C). It is important to emphasize that the striking difference in effectiveness in these two lights is associated with the spectral characteristics of the two lights and the differential effects on the cone opponent circuity (Figure 2.3D), not on melatonin effectiveness for which the two were equated.

Our goal is to develop lighting that can replace standard indoor white lighting and give people control of their circadian phase. A static blue light (like Figure 2.1D, top middle) is not an acceptable substitute for standard lighting because it must be pure blue to drive the color vision circuitry. Any added long-wavelength components that make the light whiter, cancelling the effectiveness. As an alternative, we tested a temporally modulated light because, unlike the melanopsin drive to ipRGCs, which is quite sustained, the cone inputs have transient responses. There are two types of color-opponent ipRGCs in primates, S-ON and S-OFF, but both are ON-OFF cells responding both to the onset of one colored light and the offset of the light of the opposing complementary color.[8]

Thus, theoretically, the best stimulus is a light that alternates between short and long-wavelength components such that the color-opponent cells are being stimulated by the simultaneous offset of one spectral component and the onset of the opposing component. It is possible to produce lights that, when temporally alternated, appear white but strongly modulate S-cones. The S-cone inputs to ipRGCs are tuned to respond to higher temporal frequencies than those serving hue perception, making it possible to modulate the S-cone input to ipRGCs strongly but minimize (and ideally eliminate) the percept of flicker. The S-cone modulating light tested here consisted of a 19 Hz alternating pulse train designed to modulate the quantal catch of S-cones with a differential of 100X between the two phases. This was done by alternating the intensities of LEDs peaking at 426 nm vs. 539 nm, and the addition of light from a 634 nm LED made the S-cone modulated pulse train appear nominally white. The intensity of this light was adjusted to produce a time-averaged quantal catch in melanopsin matched to the 500-lux static white light of Figure 1D, top left.

As shown in Figure 2.3D, the S-cone modulated "white light" elicited a striking 1 hr 20 min phase advance. It is important to emphasize that the striking difference in phase advance produced by this light condition has nothing to do with melanopsin activation since the time averaged effect on melanopsin was the same as the other two lights. The effect is associated with the greater temporal sensitivity of cone photoreceptor inputs to ipRGCs.

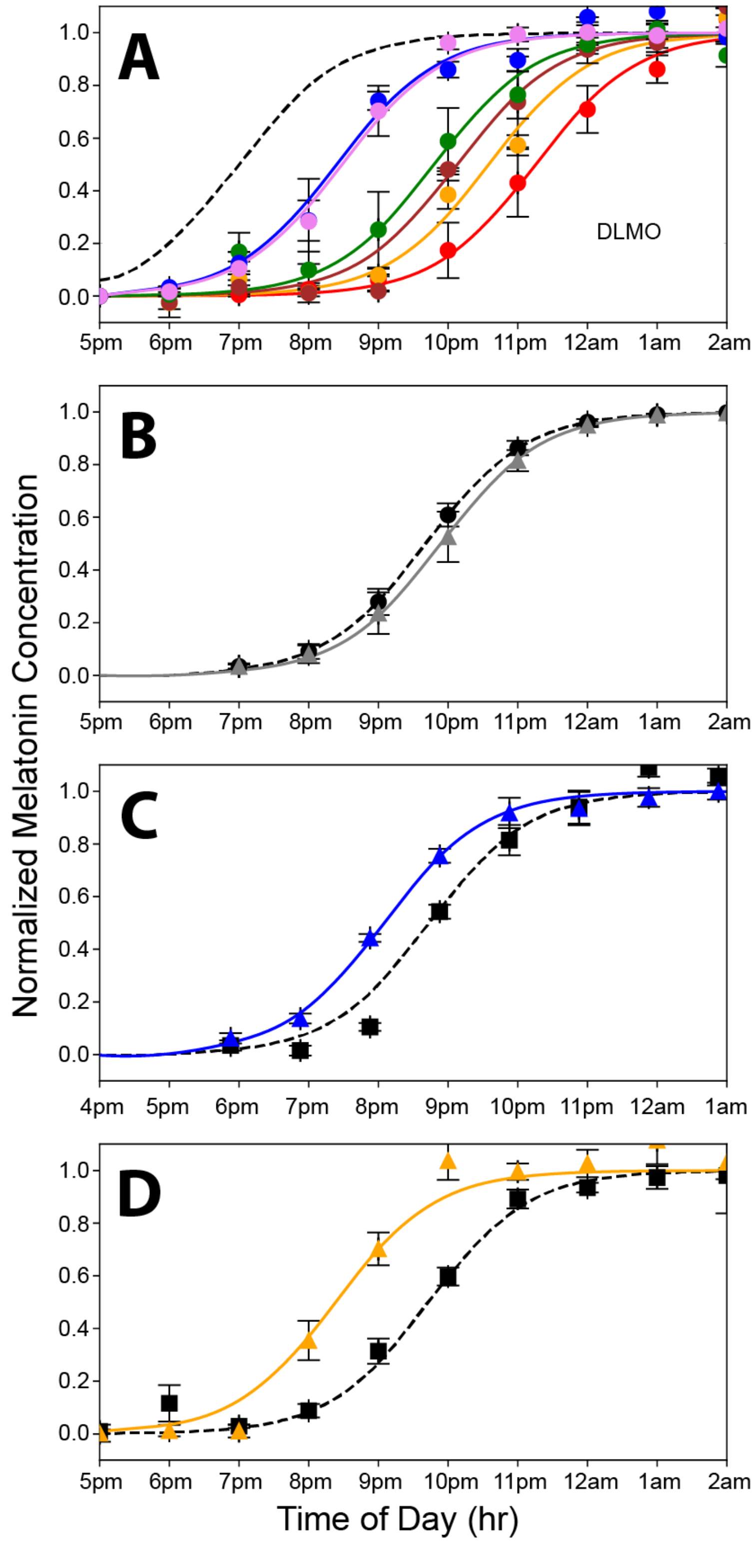

Figure 2.3 Curves showing the nighttime dim rise in salivary melatonin levels under various conditions equated for melanopsin effectiveness. **(A)** Baseline rise in evening melatonin levels for the six subjects who participated in this study (each is shown in a different color). The dashed

gray curve shows the predicted rise if the subjects were aligned to earth time where beginning of internal biological night occurs at sunset. On average, subjects were phase delayed 2.8 h. **(B)** Average rise in evening melatonin after two-hour exposure to the static white light (gray curve) of Figure 1A compared to a baseline (dashed curve) measured on day one of the 3-day protocol. There was a slight, nonsignificant, phase delay associated with the white light exposure (n=3 subjects). **(C)** Average rise in evening melatonin (blue curve) after a two-hour exposure to the 476-nm blue light of Figure 1D middle compared to baseline (dashed curve) (n=6 subjects). The 476-nm light produced a phase advance of 40 minutes. **(D)** The Rise in evening melatonin (orange curve) after two-hour exposure to 19 Hz S-cone modulated light compared to baseline (dashed curve) (n=6 subjects). This light produced a phase advance of 1 hour and 20 minutes.

2.4 DISCUSSION

Blue lights are particularly effective in driving ipRGCs[64,65], and it is often assumed this is mediated by melanopsin. However, one novel aspect of the experiments here is that the blue and white lights were equated for melanopsin effectiveness: thus, the large effect of blue compared to white cannot be attributed to activation of melanopsin. Since the white condition nulls the color-opponent response (Figure 2.1D, left), it effectively isolated the melanopsin drive to the ipRGCs. We conclude, that under the relatively low light conditions and two-hour exposure duration used here, melanopsin activation is insufficient to produce any significant circadian phase advance. Moreover, it follows that the substantial phase advance produced by the blue light equated in melanopsin effectiveness to the white light is the result of activation of the color-opponent circuitry, not melanopsin, as commonly assumed. The implication of our result reported here is that, because modest illumination level (ca. 500 lux) white lights presented for relatively short duration exposures (≤ 2 hours) are ineffective in stimulating melanopsin sufficiently to produce a phase advance, any practical indoor lighting solution to social jet lag and other problems associated with a delayed circadian clock must focus on stimulating the color opponent inputs to ipRGCs.

Previously, one hour of bright white (~10,000 lux) light produced a 40 minute advance in circadian phase.[20] When white lights are sufficiently bright, they can produce a phase advance by activating the much less sensitive melanopsin expressed in human ipRGCs compared to the 500-lux static white light that was ineffective here (Figure 2.3D). However, light that strongly modulates the S-cones for two hours (500 lux X 2 hr vs. ~10,000 Lux X 1 hr) amounts to 10X fewer lux-hours but produced a circadian phase advance per exposure hour that was twice as great. Thus, the S-cone modulating light is twice as effective as very bright white light at 1/20th the intensity.

As a different alternative to static illumination, Zeitzer et al. administered 60 2-msec pulses of 473 Lux broad spectral band light over an hour and produced a phase change nearly half that of 1-hour 10,000 Lux static white light.[25] We assume that the increased effectiveness is due to the involvement of cone circuits, as in the experiments reported here, since transient white flashes drive spectrally opponent cone inputs to ipRGCs by virtue of differences in the temporal properties of their components. However, because of the spectrally opponent nature of the cone inputs to ipRGCs, modulating S- vs. LM cones is superior to non-spectrally selective cone modulation. The S-cone modulating light is 4 times more effective, and the exchange between long and short wavelength components can be invisible whereas bright flashes every minute are not a practical alternative to traditional illumination.

Earlier, Spitschan and colleagues[66] measured melatonin suppression using two light stimuli that differed exclusively in the amount of S-cone excitation by almost two orders of magnitude, but not in the excitation L and M cones, rods, and melanopsin. Since the light with stronger S-cone excitation did not differentially suppress melatonin, it might be interpreted to suggest a lack of support for a role for S-cone signals in circadian phototransduction. However, the Spitschan et al.

experiment relies on the assumption of additivity which doesn't apply to color opponent systems. As shown here, static white lights can produce strong S-cone excitation but provide zero drive phase advances mediated by ipRGCs because of the opponent nature of the cone inputs. The "S cone isolating light" used by Spitschan was a pinkish color compared to "S- light" which was orangish. This is because to equate the two lights for L and M effectiveness the S+ light had to include about equal amounts of long and short wavelength light, nulling the color opponent response much like what occurs with the white light, as illustrated in Figure 1D, left. Thus, the results reported here are consistent with those of Spitschan et al., showing that lights with strong S-cone excitation (a white light in our case and a pink one for Spitschan et al.) that balance S and (L+M) activation don't have strong effects. In addition, our results are consistent with more recent studies which show that color opponent circuitry is involved in circadian phototransduction.[24,58]

The color of the sky at sunrise and sunset (Figure 2.1C) is the ideal cue for synchronizing one's internal body clock to solar time. The intensity of light overhead can vary greatly for many reasons, making it an unreliable indicator of the time of day, but the orange color of the sky at the horizon always indicates that it is sunrise or sunset. Retinal ganglion cells act as feature detectors. The color opponent inputs to ipRGCs confer the ability to act as sunrise/sunset detectors. The orange color of the horizon that characterizes the rising and setting sun produces a color contrast with the blue sky (Figure 2.1C). The blue and orange parts of the image on the retina produced by the sunset moving across the receptive field of an ipRGC activates the transient color-opponent response very strongly. As shown in Figure 2.1A, when our internal clock is aligned with solar time, sunrise occurs after the peak of the phase advance portion of the phase response curve, and sunset occurs before the peak of the delayed phase portion. When the ipRGCs are strongly stimulated at both dawn and dusk, the human phase response curve is perfectly tuned to keep the phase of our internal pacemaker precisely aligned with solar time.

Color opponent mechanisms are associated with sensory systems that regulate circadian activity throughout the animal kingdom including fish and reptiles.[67,68] Ancient single-celled organisms exhibit color sensitivity that they use to regulate their circadian activity.[69] It appears that the capacity to sense colors originally evolved to serve circadian rhythms, not for hue perception.[70] The fact that primates have evolved multiple independent circuits that provide color-opponent inputs to ipRGCs is a testament to the importance of these sunrise and sunset detectors to our evolutionary survival. Thus, it makes perfect sense to develop lighting to use these color vision circuits to take control of our circadian wellbeing.

Our goal is to take control of our circadian rhythms by adding light exposures that strongly modulate S-cone opponency in the morning in the context of the light experience in people's regular daily lives. Thus, here, each subject was exposed to the experimental lights on a background of their regular daily lives as academics at the University of Washington. In this context, exposure to a 500-lux static white produced no significant phase advance, but a light with the same melanopsin effectiveness that temporarily modulated S-cone color opponent circuitry produced phase advances, that if administered in the context of a person's normal lighting routine, would be capable of offsetting the average 2.8-hour delay, therefore eliminating social jet lag.

The discoveries of color vision circuitry inputs to primate ipRGCs[13,14], together with the evidence that has accumulated showing the role that circuitry in circadian phototransduction, indicate the need for a complete paradigm shift in the strategy to develop healthy circadian lighting away from focusing on melanopsin to emphasizing the cone inputs. Melanopsin might have been emphasized over the powerful effects of the color-opponent inputs to ipRGCs because ideas about resetting of phase in humans have been extrapolated from experiments on rodents that have emphasized melanopsin. While it has been recognized that ipRGCs could be activated by classic photoreceptor input in the absence of melanopsin in mice[4], neither M1 nor M2 ipRGCs in mice were reported to have inputs from the color-opponent circuitry observed in primates[71,72]; however, more recently, differential inputs between S and M cones were shown to produce responses in the suprachiasmatic nucleus of mice, recognizing the importance of cone inputs for circadian entrainment, especially in cone dominated species.[5] Here, we demonstrate that, rather than focusing on melanopsin under the constraints of making lights that appear white with intensities like standard artificial lighting used indoors, stimulating ipRGCs by modulating S-cones has promise to give people control of their circadian rhythms to improve mood, sleep, and health.

Chapter 3. SCN-VIP NEURONS UNDERGO A DAILY CYCLE OF RETRACTION AND GROWTH

3.1 INTRODUCTION

In mammals, overt circadian rhythms of physiology and behavior are centrally regulated by a circadian clock located in the suprachiasmatic nucleus (SCN) of the hypothalamus. The fact that the SCN has only about 10,000 neurons points to a remarkable localization of function by which 24-hour (h) rhythms as diverse as the sleep-wake cycle, cognitive performance and hormonal release are regulated. The ability of the SCN to function as a robust tissue circadian pacemaker relies on several of its properties. First, both SCN glia and neurons express so-called clock genes. The expression of these genes interacts in a transcription-translation feedback loop (TTFL) that leads to the cell-autonomous 24-h rhythms of their expression.[73] The TTFL has the ability to relay its rhythmicity to the expression of "clock-controlled genes" whose expression results in cell-specific rhythms. These rhythms involve 24-h oscillations in the resting potential and firing rate of neurons, as well as changes in the release and receptor machinery of neuropeptides and classic neurotransmitters.[73,74] Second, SCN cells interact within a network that is exquisitely tuned to generate robust 24-h rhythms. Indeed, isolated SCN neurons, or SCN neurons cultured at low densities where their typical interactions are impaired, are weak single-cell oscillators.[75] Conversely, SCN slices from mice missing clock genes that impair the TTFL function can display 24-h rhythms of gene expression that clearly result from emergent SCN network properties.[34] Third, SCN afferent and efferent connections are critical to its function as central circadian pacemaker. Direct axonal projections from retinal ganglion cells reach the SCN to convey photic information that is critical to entrain the nucleus—and all the rhythms it regulates—to the LD cycle.[76] In turn, the SCN conveys circadian signals to the rest of the brain through the release of humoral factors as well as through efferent projections to specific brain regions; these outputs can directly—or indirectly through the synchronization of extra-SCN circadian oscillators—sustain overt circadian rhythms.[28,77-79]

The SCN is constituted by phenotypically diverse neurons that synthesize different neuropeptides and transmitters, and display different 24-h rhythmic patterns of gene expression.[30,80] This heterogeneity is critical for the SCN coding of photic input, maintenance of network properties and output control. Notably, a subset of neurons that synthesize vasoactive intestinal polypeptide (VIP) are unique in that they play key roles in all three functions: They are critical for modulating the coding of photic input to the SCN,[81,82] maintaining rhythm coherence within the neuronal network,[43,44,46] and sustaining the circadian rhythms of locomotor activity, glucocorticoid release[28] and the daily siesta that mice display in the middle of night.[29] VIP is the only neuropeptide signal whose absence has such a drastic effect in both the pacemaker and the behavioral rhythms it regulates.

The mechanisms by which VIP neurons can play these diverse and central roles in the SCN are not completely understood. All VIP neurons are GABAergic[26,30], and some of the VIP neuron functions rely on the release of GABA.[39] On the other hand, daily application of a VIP agonist on arrhythmic SCN slices from VIP KOs rescues the circadian rhythm of electrical activity[46], clearly pointing to the ability of VIPergic signaling to regulate a coherent output from the SCN cellular network, and suggesting that part of the VIPergic neuron function relies on the 24-h rhythmic synthesis and release of the peptide. This interpretation is consistent with the diurnal pattern of *Vip* mRNA expression[83-86] and the expression and release of VIP.[87,88]

Interestingly, immunohistochemical studies in the rat have shown a 24-h rhythm of VIP fiber immunoreactivity under LD conditions, a finding that has been interpreted as the result of a daily rhythm in the peptide's synthesis, transport and/or release.[88] An alternative explanation for this result is that the change in VIP immunoreactive fibers is the consequence of a daily rhythm of growth and retraction of VIPergic fibers. Such a rhythm could underlie dynamic 24-h changes in photic sensitivity, neuronal connectivity and output signals. 24-h structural plasticity changes that involve the formation and elimination of synapses have been shown in the central circadian clock of *Drosophila*[89], and the mechanisms underlying these changes are beginning to be elucidated[90-100]. This "circadian structural plasticity" has apparent functional implications, as it is associated with changes in the quantity of active zones, changes in connectivity and even switches on the synaptic partners of pigment-dispersing factor (PDF)-containing clock neurons.[101,102] Furthermore, when this plasticity is disrupted, normal circadian entrainment appears to be disrupted.[103] PDF-containing neurons are central to the function of the *Drosophila* central circadian clock, and these findings led us to hypothesize that circadian structural plasticity may represent a signature feature of central neuronal circadian pacemakers. SCN VIPergic neurons are functionally analogous to the fly's PDF-containing neurons, and to test this hypothesis we here examine whether SCN VIPergic fibers undergo 24-h rhythms of growth and retraction.

Previous work assessing VIPergic fiber density changes have two limitations.[88] First, VIP immunoreactivity under light or fluorescent microscopy cannot distinguish neuronal processes that grow and retract from neuronal processes that show changes in the amount of VIP within fibers. Second, thin sectioning—30-40 μm—required for classic immunohistochemical techniques makes the comparison of fiber staining between animals highly error-prone; i.e. a minor difference in the slicing angle leads to large apparent changes in SCN fiber density. To circumvent these two technical limitations, first, we used a mouse transgenic line that expresses cytoplasmatic tdTomato within VIPergic neurons, allowing for the visualization of neuronal processes regardless of the subcellular localization of VIP. Second, we used a tissue-clearing technique that allows the visualization of the whole SCN, including the totality of VIP neurons and their processes in single 500-µm-thick slices.

3.2 METHODS

3.2.1 *Animals*

All experiments were performed with approval from the University of Washington Institutional Animal Care and Use Committee. Homozygous VIP-IRES-Cre knockin mice (*VIP$^{tm1(cre)Zjh}$/J*; The Jackson Laboratory catalog #010908)[104] were crossed to homozygous Lox-Stop-Lox-tdTomato knockin mice (B6.Cg-*Gt(ROSA)26Sor$^{tm14(CA\text{-}tdTomato)Hze}$/J*; The Jackson Laboratory catalog #007914)[105] to get VIP-Cre$^{+/-}$-flox-stop-flox-tdTomato$^{+/-}$ mice on C57BL/6 background, which express tdTomato fluorescent protein in VIP neurons. Mice were housed in a 12:12 hour LD cycle with up to 5 mice per cage. For constant darkness experiments, the lights were removed during the dark phase. Mice were kept in constant darkness for the entirety of the following 24 hours and then sacrificed in the next cycle. Circadian Time of sacrifice was estimated from the prior LD cycle. Mice were between 6-16 weeks of age at the time of sacrifice. Mice were housed with *ad libitum* food and water, and constant temperature and humidity for the entirety of the experiment.

3.2.2 *Female estrus phase determination*

Phase of estrous was determined by vaginal opening as previously reported.[106]

3.2.3 *Tissue clearing*

Mice were anesthetized with an overdose of isoflurane then transcardially perfused with PBS to flush the blood vessels followed by 4% PFA in PBS for fixation. The brains were dissected and post-fixed in 4% PFA in PBS for 24 hours. The brains were washed in PBS and a 700 µm coronal section containing the SCN was blocked. The sections were further washed in PBS. The sections were treated with delipidation reagent CUBIC-L (TCI chemicals #T3740) at 37°C for 3 days. If the brains were not treated for immunohistochemistry, they were immediately moved to RI matching reagent CUBIC-R+ (TCI chemicals #T3741) diluted to 0.5X in water for 1 day followed by 1X CUBIC-R+ until imaging.

For immunohistochemistry with tissue clearing, a published protocol was followed.[107] Brains were washed with PBS 3 times for 30 min at 37°C. Two µg of primary antibody were mixed with 1.5 µg of secondary antibody and incubated at 37°C for 1.5 hours. The brain slices were incubated in HEPES TSC (10mM HEPES, 10% Triton X-100 (v/v), 200 mM NaCl, 0.5% casein) for 1.5 hours at 32°C. HEPES-TSC was added to the antibody mixture to a total volume of 300 µL. The brain slices were immersed in 300 µL of the antibody mixture at 32°C for 1 week, followed by 1 day at 4°C. The brains were washed in 0.04% PBST for 30 min 2 times at room temperature (~20°C). The brains were washed in PBS for 1 hour at room temperature. The brains were post-fixed in 1% formaldehyde in PBS for 1 day at room temperature. The brains were washed in PBS for 2 hours at room temperature. The brains were immersed in 0.5X CUBIC-R+ for 1 day, followed by 1X CUBIC-R+ until imaging. (Primary antibodies: Rabbit anti-Vgat (Genetex GTX101908), Secondary antibodies: Fab fragment Alexa 647 Goat anti-Rabbit (Jackson 111-607-008)).

3.2.4 *Imaging*

A Nikon A1R scanning laser confocal was used to acquire all images. For images of VIP fibers that were non-immunostained (i.e. brains only containing native tdTomato fluorescence), a Plan Apochromat Lambda 20x (NA 0.75, WD 1.0 mm) objective at 1X zoom were used. For images acquired of VIP cell bodies, the zoom was increased to 2X. For immunostained brains, images of the entire SCN were acquired with a Plan Apochromat Lambda 10× (NA 0.45, WD 4.0 mm) objective at 2X zoom. Z section thickness was 3 μm for all analyzed images.

3.2.5 *Analysis*

To calculate the area covered by VIP fibers or by Vgat positive puncta in the SCN, the images were made binary such that each pixel was labeled either background or fiber. This was done by training machine learning algorithms with the software QuPath [108]. To train the VIP fiber algorithm, several images were densely annotated. Annotations were labeled either background or fiber. To validate the algorithm, several images from different experimental conditions (e.g. different timepoints and sexes) that were not used to train the algorithm were densely annotated. The human annotations were compared against the algorithm. The percent true fiber detection was 75%, and the percent true background detection was 77%. Due to variability in the Vgat IHC images, individual algorithms were trained for each image. These algorithms were validated by comparing the annotations that were used to train them against the machine learning output. All of the Vgat algorithms had percent positive Vgat detection rate and percent positive background detection rate of >98%.

To calculate the area covered by VIP fibers across the different SCN regions, thin ROIs (10 pixels) were made either from the right to left of the image or from the top to bottom of the image on each coronal section (Figure 3.1). The fiber density from the same ROIs across each coronal Z slice were summed.

3.2.6 *Statistics*

Data analysis was performed blind to time of sacrifice. All statistics were performed in Python using the scipy stats package or using statsmodel package.

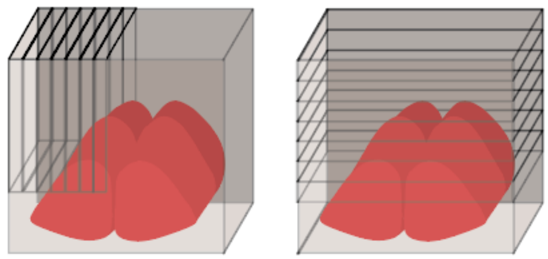

Figure 3.1 Calculating fiber density across regions of interest. Thin regions of interest were made either top to bottom or left to right in order to make quantifications across the lateral to medial axis (left) and dorsal to ventral axis (right).

3.3 RESULTS

To test the hypothesis that VIP neurons undergo daily cycles of retraction and growth, we obtained images of VIP neurons from *VIP-Cre$^{+/-}$-flox-stop-flox-tdTomato$^{+/-}$* (mice that express cytosolic tdTomato only in VIP-expressing neurons; from here onwards *Vip-Cyt-tdTomato*) male mice euthanized at different times throughout a 12:12 hour L:D cycle. We obtained images from a tissue-cleared brain block containing the SCN and extending outside the SCN (Figure 3.2A), and made the tdTomato fluorescence images binary with a machine learning algorithm in the software QuPath (Figure 3.2B). Each pixel was either labeled as part of the VIP neuron or background. This analysis was performed only in regions where VIP cell bodies are not located. Therefore, all VIP neuron-positive pixels represented neurites. We found that the VIP neurites occupy more space during the day compared to night (Figure 3.2C, Student's t-test, statistic=3.56, p=0.0009), with a 34.3% decrease from day to night. The fiber density of the VIP neurons reached a peak at ZT3 (Figure 3.2D, One Way ANOVA, $F_{(7,36)}$=3.82, p=0.003).

We next asked if the differences we found in the entire brain block in retraction and growth were region-specific. To do this, we looked at the images across the three axes: coronal, horizontal, and sagittal. Then we examined each part of the brain block from rostral to caudal, dorsal to ventral, and lateral to medial (Figure 3.3A, B). We found significant changes across all coronal and horizontal sections (Figure 3.3C-H). However, along the sagittal axes we detected significant changes in the central and medial regions, but not in the lateral region (Figure 3.3I-K). This indicates that the fibers are extending and retracting dorsoventrally and rostrocaudally, but are not migrating laterally.

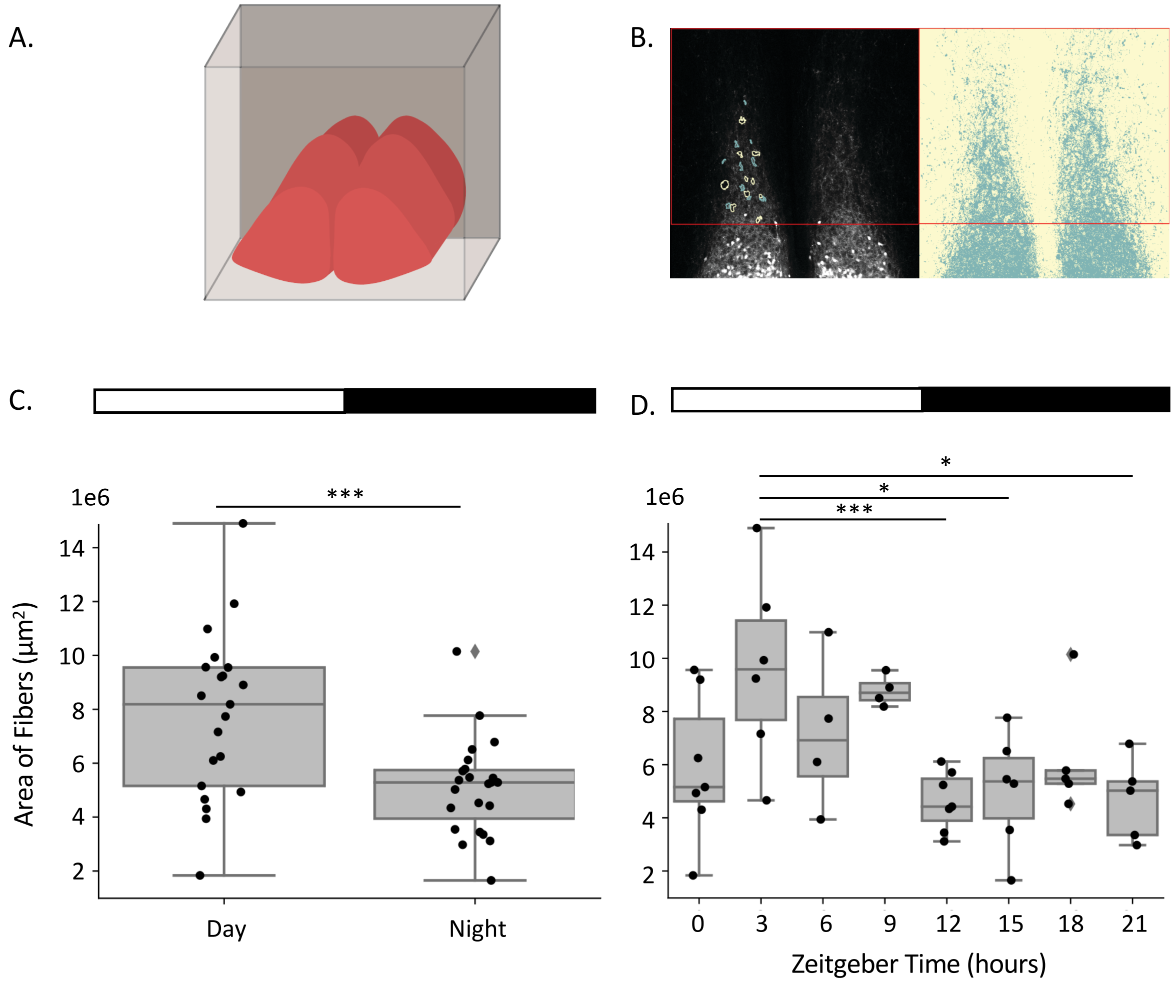

Figure 3.2 VIPergic neuronal processes in the SCN grow and retract across the light-dark cycle in male mice. A.) Cartoon representing the region of interest. VIP neurite area was measured from this entire volume, excluding the most ventral region containing cell bodies. B.) The raw image of cytosolic tdTomato fluorescence in VIP neurons was annotated for either VIP neurites or background (left). The annotations were used to train an algorithm that made the image binary (right, blue represents VIP neurites, yellow represents background). The red outline indicated the region that was measured. C.) The area of VIP neurites from binary images as in B. was quantified in volumes from mice sacrificed at ZT 0, 3, 6, and 9 and data were binned into Day, while data from mice sacrificed at ZT 12, 15, 18, and 21 was binned into Night (Student's t-test, statistic=3.56, $p=0.0009$, $n_{day}=21$, $n_{night}=23$). D.) Unbinned data from C (One-way ANOVA, $F_{(7,36)}=3.82$, $p=0.003$, ($n_0=7$, $n_3=6$, $n_6=4$, $n_9=4$, $n_{12}=7$, $n_{15}=6$, $n_{18}=5$, $n_{21}=5$). Tukey's post-hoc comparisons *$p<0.05$, **$p<0.01$, ***$p<0.001$

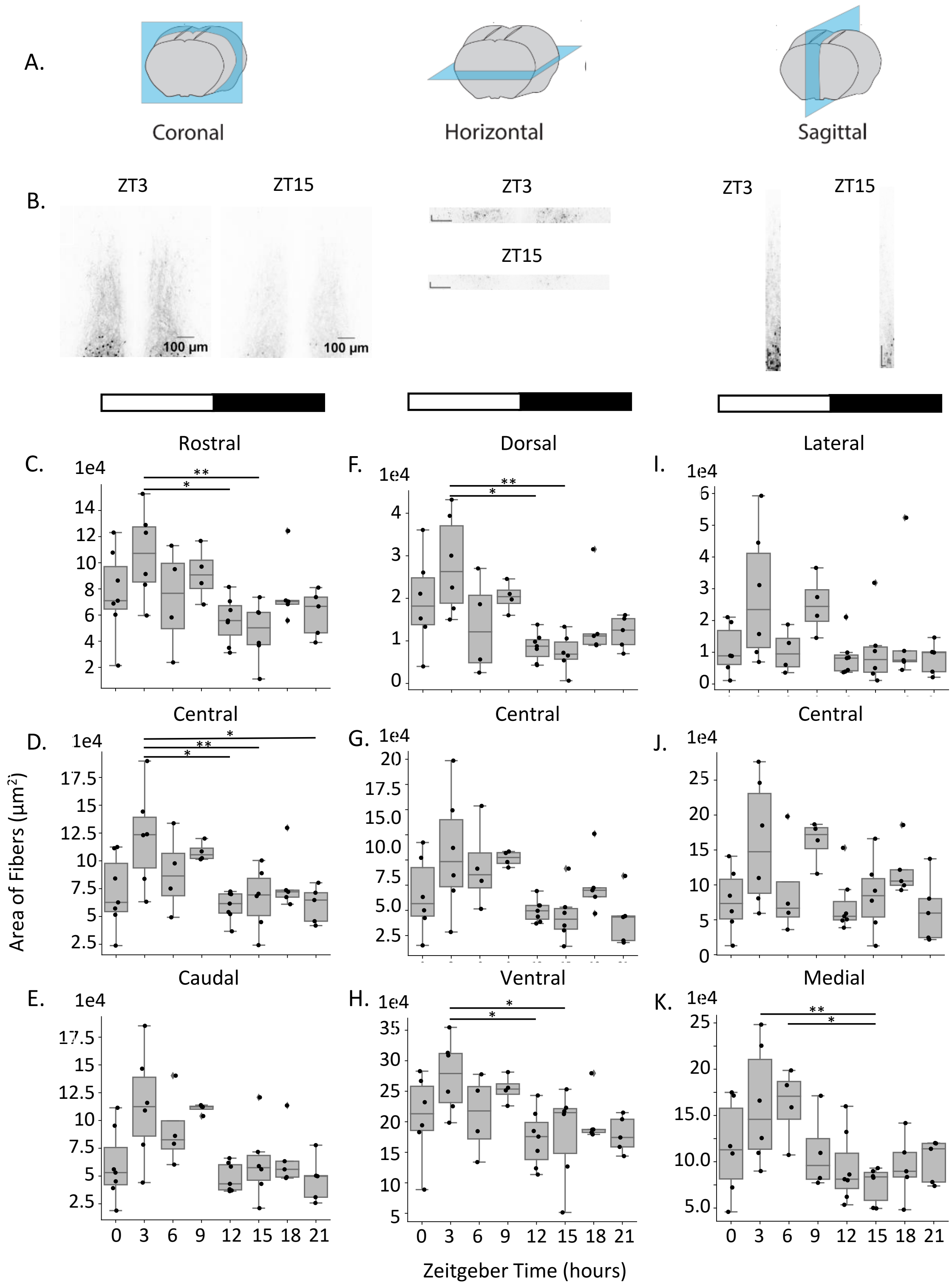

Figure 3.3 VIPergic neuronal processes in the SCN grow and retract in specific regions. Each column represents data along one axis. C-E represents the caudal axis, F-H represents the

horizontal axis, and I-K represents the sagittal axis. A.) Cartoon representing the axes across which the data is analyzed. B.) Representative confocal images from rostral (left), dorsal (middle), and medial optical slices (right) of cleared SCN tissue from a mouse euthanized at ZT3 and a mouse euthanized at ZT15. All scale bars represent 100 μm. C-K.) VIP neurite area in specified regions (n_0=7, n_3=6, n_6=4, n_9=4, n_{12}=7, n_{15}=6, n_{18}=5, n_{21}=21). C.) One-way ANOVA, $F_{(7,36)}$=3.22, p=0.009. D.) One-way ANOVA $F_{(7,36)}$=3.7, p=0.004. E.) Kruskal-Wallis $\text{statistic}_{(7,36)}$=18.2, p=0.01. F.) $\text{Kruskal-Wallis}_{(7,36),}$ statistic=20.9, p=0.019. G.) Kruskal-Wallis, $\text{statistic}_{(7,36)}$=17.7, p=0.013. H.) One-way ANOVA, $F_{(7,36)}$=2.62, p=0.027. I.) Kruskal-Wallis, $\text{statistic}_{(7,36)}$=11.9, p=0.1, J.) One-way ANOVA, $F_{(7,36)}$=2.66, p=0.025. K.) One-way ANOVA, $F_{(7,36)}$=3.34, p=0.0076.

Tukey's post-hoc comparisons *p<0.05, **p<0.01, ***p<0.001

Next, we analyzed whether VIP neurites retract and grow across the day in female mice. We binned female data from multiple day time points (ZT0 and 3) and night time points (ZT12 and 15). We found females displayed statistically significant differences between day and night (Figure 3.4B, Student's t-test, statistic=2.047, p=0.048) with a 22.2% decrease in fiber density from day to night. Considering the effect size is smaller in female mice (Figure 3.4A, B), a two-way ANOVA was performed to analyze the effect of time and sex on the area that VIP neurites occupy (Table 3.1). The male data were binned into day and night time points for comparison (day=ZT0 and 3, night=ZT12 and 15). There was a statistically significant interaction between the effects of time and sex (two-way ANOVA, p=0.0079). Simple main effects analysis showed that neither time nor sex had a statistically significant effect on VIP neurite density (two-way ANOVA, p=0.066 for time, p=0.7 for sex). The interaction between time and sex may be due to differences in levels of sex hormones. Indeed, when we only analyzed data from mice in metestrus, the effect size increased (53% decrease, Student's t-test, statistic=2.8, p=0.049).

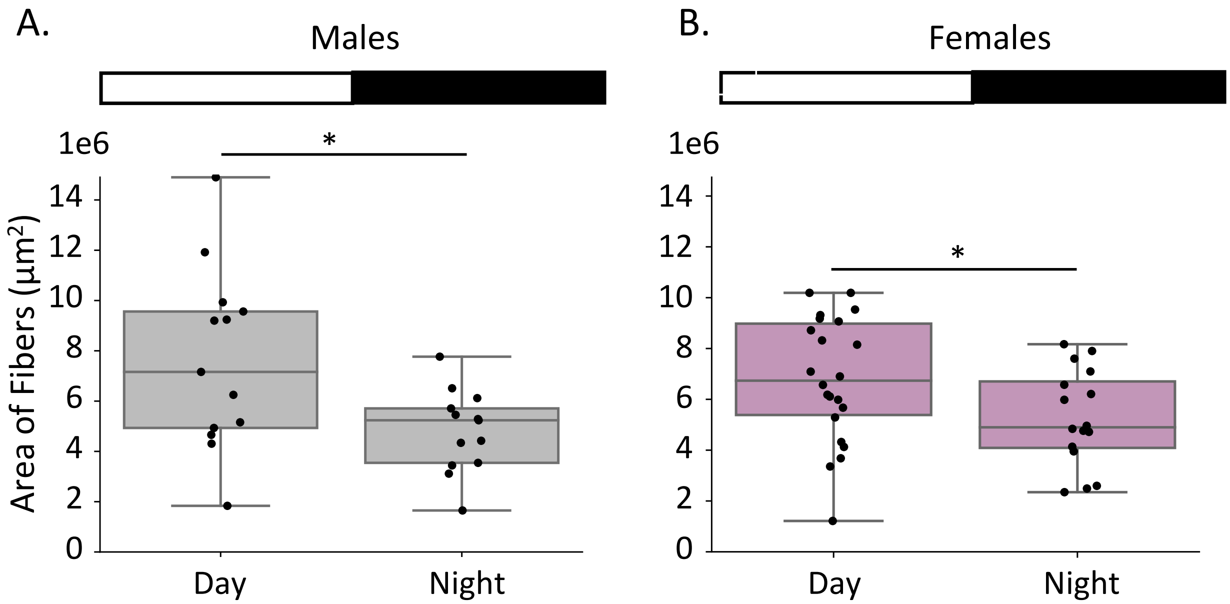

Figure 3.4 VIPergic neuronal processes in the SCN grow and retract across the day-night cycle in male and female mice. A.) Data for male mice are identical to Figure 1C. (Student's t-test, statistic=3.56, p=0.0009, n_{day}=21, n_{night}=23). B.) Female mice (Student's t-test, statistic=3.56, p=0.0009, n_{day}=26, n_{night}=24).

Table 3.1. Two-way ANOVA results for the interaction between time and sex on VIP neurite retraction and growth

	Degrees of Freedom	SS	MS	F	p-value
Time	2	3.32E+13	1.66E+13	2.891234	0.066359
Sex	1	8.52E+11	8.52 E+11	0.148386	0.701981
Interaction	2	6.23E+13	3.12E+13	5.430532	0.007892
Residual	43	5.74E+12	5.74E+12		

Next, we asked whether the changes in VIP neurite retraction and growth were regulated by the circadian clock. Male *VIP-Cyt-tdTomato* mice were housed in a 12:12 hour LD cycle and then exposed to one complete cycle of total darkness. Mice were euthanized at circadian times 3 (CT3, 3 hours after the extrapolated lights-on time) and CT15 because these were the peak and trough under LD conditions. We found that the effect was dampened in constant darkness (Figure 3.5, student's t-test, statistic=1.08, p=0.307), suggesting neurite retraction and growth represent an acute effect of the light-dark cycle. It is possible that the phase shifted after the lights were turned off, contributing to a smaller and statistically undetectable effect. However, this is unlikely since the lights were only off for one cycle. A two-way ANOVA with light condition and time as main effects (Table 3.2) showed that time had a significant effect (p=0.013), but light condition did not (p=0.93). There was no significant interaction between light condition and time (p=0.26).

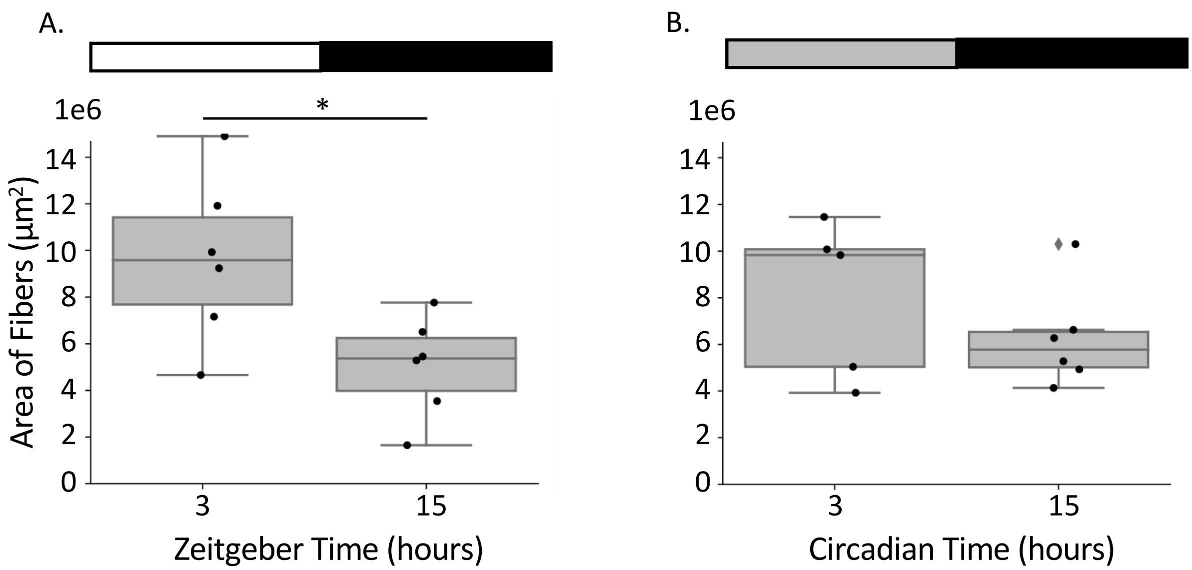

Figure 3.5 VIPergic neuronal processes in the SCN do not grow and retract in constant darkness. A.) Male mice in a 12:12 hour light dark cycle (Student's t-test, statistic=2.69, p=0.023, n_3=6, n_{15}=6). B.) Male mice in constant darkness (Student's t-test, statistic=1.08, p=0.031, n_3=5, n_{15}=6).

Table 3.2. Two-way ANOVA results for the interaction between time and light condition on VIP neurite retraction and growth

	Degrees of Freedom	SS	MS	F	p-value
Time	1	6.16E+13	6.16E+13	7.488527	0.013112
Light Condition	1	6.49E+10	6.49E+10	0.007885	0.930173
Interaction	1	1.11E+13	1.11E+13	1.350563	0.25957
Residual	19	1.56E+14	8.23E+12		

In the *VIP-Cyt-tdTomato* mouse line, the fluorescent protein tdTomato fills the entire VIP neuron, so it is not possible to distinguish whether the retraction and growth involve dendrites, axons or both. To distinguish this and considering that virtually all VIPpergic SCN neurons are also GABAergic, we performed immunohistochemistry against the vesicular transporter for GABA, Vgat, on tissue-cleared SCN slices from *VIP-Cyt-tdTomato* male mice euthanized at ZT3 and ZT15 (Figure 3.6A). We quantified the overlap between the Vgat and tdTomato to get the total area that putative presynaptic VIP fibers occupy at different times of the day. As expected, VIP neurites retract and grow across the day (Figure 3.6B, Student's t-test, statistic=2.82, p=0.022). The space occupied by overall Vgat-immunostained fibers did not change across the LD cycle (Figure 3.6C, Student's t-test, statistic=2.86, p=0.78). On the other hand, VIP-specific Vgat^{+} positive fibers showed a trend to occupy more space during the day compared to night, but the difference was not significant (Figure 3.6D, 21.9% decrease, Student's t-test, statistic=1.72, p=0.12).

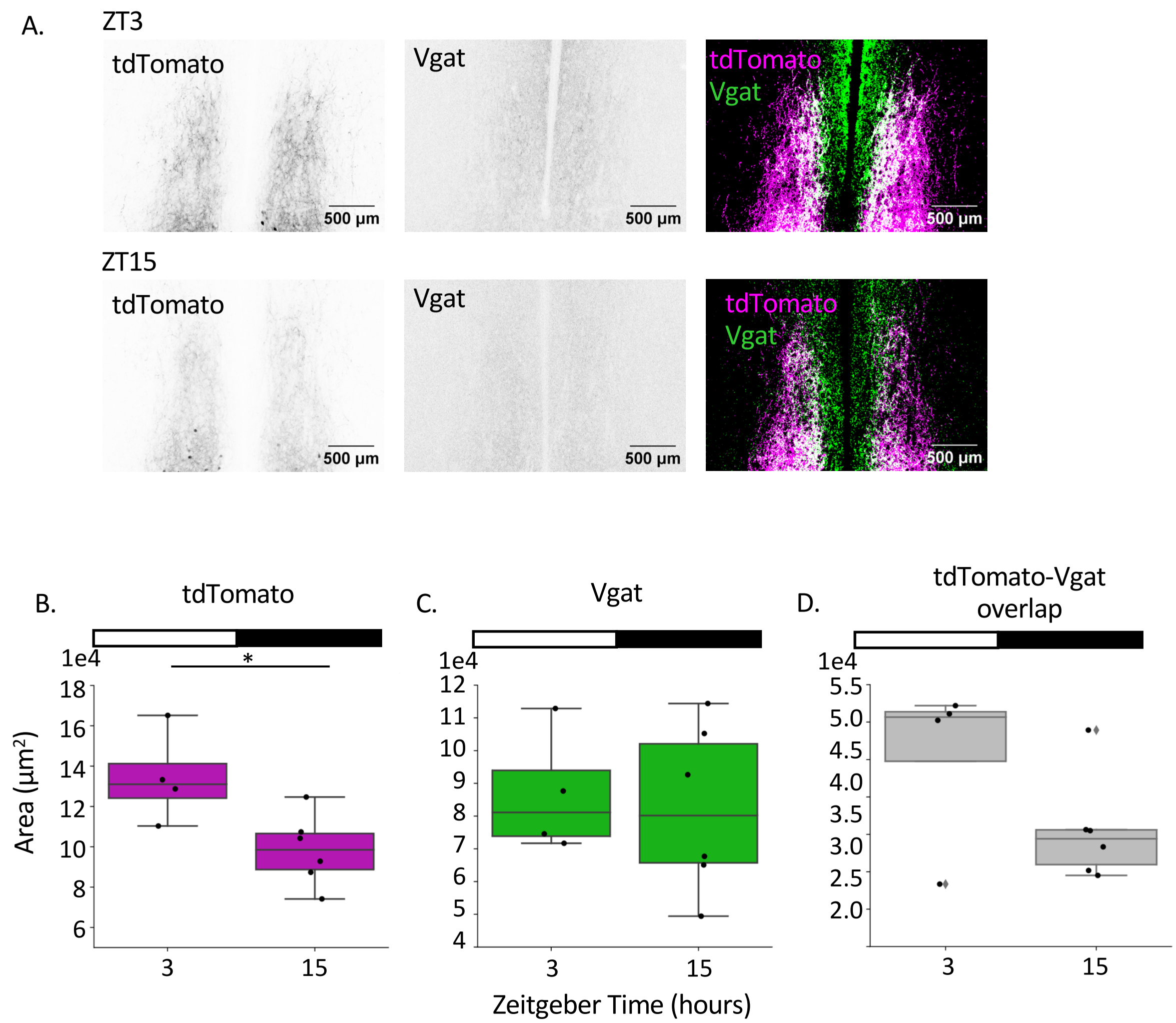

Figure 3.6 VIP neuron retraction and growth are associated with changes in the presynaptic marker Vgat in the rostral SCN. A.) Representative confocal images of cytosolic tdTomato in VIP neurons, Vgat immunohistochemistry, and binarized overlap between the two. B.) Area of cytosolic tdTomato in VIP neurons (Student's t-test, statistic=2.82, p=0.022, n_3=4, n_{15}=6). C.) Area that the Vgat occupies (Student's t-test, statistic=2.86, p=0.78, n_3=4, n_{15}=6). D.) The area of the overlap between tdTomato and Vgat (Student's t-test, statistic=1.72, p=0.12, n_3=4, n_{15}=6).

3.4 DISCUSSION

We show that VIPergic neurites in the mouse SCN show a 24-h rhythm of extension and retraction under LD conditions. This result indicates that the rhythm in VIPergic fiber immunoreactivity previously described in the rat [88] may be in part the result of daily structural changes in VIP neurons. This interpretation is further supported by the fact that, like the rhythm of immunoreactivity in the rat[88], the extension/retraction rhythm we describe dampens under constant light conditions. Together these results support the hypothesis that daily changes in fiber density of VIP neurons may represent part of the mechanisms by which the SCN codes photic information. Although the functional implications of daily structural changes in the SCN remain to be determined one obvious implication should be changes in synaptic connectivity. Interestingly, previous studies in rats showed that VIP neurons receive more synaptic contacts during the day compared to night[53], but the mechanism behind these changes remain unknown. Our results provide a novel mechanism that could underlie these changes.

In *Drosophila*, neurons within the small lateral neuron cluster constitute the central circadian oscillator. A subset of these neurons that express PDF, a peptide analogous in function to SCN VIP, are more branched during the day than the night[89]. In flies, the rhythm is driven by the circadian clock and persists in constant conditions. In contrast, our results suggest the growth-retraction rhythm in SCN VIPergic neurons is dependent on the presence of the LD cycle. In constant conditions, the subjective day measurements of VIP neurite area were lower, and the subjective night measurements were higher compared to the samples taken during a LD cycle, suggesting that the LD cycle drives the amplitude of the rhythm. An alternative explanation is that the similar values of fiber density observed under constant darkness conditions represents a sudden phase shift in the 24-h rhythm. This latter interpretation seems unlikely given that the animals were euthanized 24 h after their release into constant conditions.

Studies in *Drosophila* have provided the first hints to the putative function of circadian structural plasticity. As predicted, circadian structural changes are associated with changes in the number of active zones and, remarkably, with changes in the synaptic partners that PDF neurons have across the day[39] . Interestingly, when circadian structural plasticity of the PDF neurons is eliminated throughout development the manipulation has no detectable effects on circadian rhythmicity, although it appears to affect entrainment to ambient temperature cycles[103].

Experiments in the rat showing changes in synaptic input[53] and VIP immunoreactivity[88] did not include females. In our study, VIP neurites in female mice extend and retract across the day-night cycle: however, the effect size is smaller than that of males. In other brain regions, phase of estrous affects structural plasticity.[109] For example, spine and synapse density in the hippocampus is higher at proestrus than estrous.[110,111] It is likely the differences between sexes we report are caused by differences in circulating sex hormones. Consistent with this interpretation, we found that the magnitude of day-night VIP neurite changes in females were most similar to males during metestrus, the phase in which circulating sex hormones are at their lowest. Intriguingly, SCN neurons express no estrogen receptor (ER)-a although they may express low levels of ER-b (reviewed in [112]). The sex differences may be due to differences in upstream input to VIP neurons, or due to differences in other sex hormones such as progesterone.

We predicted that the neurite growth-retraction rhythm we observed in VIP neurons would be associated with similar changes in the area covered by their presynaptic terminals. We found that the area of VIP GABAergic synapse coverage tended to be higher during the day than at night, however the difference was not significant. The data contained two outliers, one from each group, and more data points need to be added to both groups. Confirming this trend would imply that presynaptic fibers of VIPergic neurons are changing the number of active zones they are engaged in and changing the route of information across the day-night cycle. On the other hand, growth-retraction rhythm with a relatively constant number of synapses could be causing other functional changes, such as the site of release of neuropeptides. Finally, shape changes alone can shift the electrical properties of neurons and thus alter the way in which they process and pass on information to other cells.

In conclusion, SCN VIPergic fibers retract and grow across the day-night cycle, reaching a peak in branching in the first half of the daytime. This daily rhythm likely depends on the direct effects of the LD cycle and has a lower amplitude in females, implicating a role for sex hormones. Although the functional significance of the VIPergic growth-retraction rhythm remains to be determined, our results support the hypothesis that 24-h structural plasticity may represent a defining feature of central neuronal circadian pacemakers.

Chapter 4. RESCUING THE BLUE-CONE GENE DEFECT IN HAMSTERS TO UNDERSTAND ITS WIDESPREAD OCCURANCE IN MAMMALS

4.1 INTRODUCTION

The short wavelength sensitive (S) opsin genes (*Opn1sw*) of a wide variety of mammals have accumulated mutations that render these animals devoid of S-cones.[113] This alteration reduces these species to have a single cone type making them color-blind. Different *Opn1sw* mutations have been identified in each of several species. The first mammals found to have *Opn1sw* opsin pseudogenes, the owl monkey, and the bushbaby, are strongly nocturnal primates.[114] All the terrestrial mammals later discovered to have disabling S-cone mutations are also classified as being nocturnal.[113] The list is considerable including raccoons, kinkajous, many species of bats, Syrian hamsters, and flying squirrels. Thus, there is, at least, a correlation between a nocturnal lifestyle and loss of S cones.

The animals that have lost their S-cones resemble humans that have tritan color vision defects. Tritanopia in humans is caused by a variety of mutations, and not only are the S-cones non-functional, but they also degenerate.[115] For humans, tritanopia occurs as a result of rare mutations. In contrast, in the case of the animals with S-cone mutations, the inactivated genes exist as a species trait. Moreover, as far as we know, all the animals in a given species have the same S-cone disabling mutation. However, all the different species have different mutations, so the inactivation of S-cones has evolved many times independently. Even the owl monkey (a New World Primate) and the bushbaby (an Old World Primate) have different S-opsin mutations, indicating that the loss of S-cones occurred independently.[114] The mutation has been fixed in the different populations (is homozygous for all members of the population), presumably occurring in a founder and then spreading to the entire species. Mutations undergo fixation by spreading through the population by random genetic drift or positive selection. However, the fact that the mutations have arisen in so many different species by convergent evolution and that the species share nocturnality strongly indicates that the loss of S-cones is the result of positive selection by conferring a selective advantage in these animals that relates to their nocturnal activity pattern. This is particularly interesting, in light of what was presented in **Chapter 2**[116], that the cone inputs to ipRGCs are spectrally opponent with S-cones subtractively compared to middle and long wavelength cones.[8,13,14]

Our question is what is the advantage for nocturnal species to lose their S-cones. Therefore, our goal was to restore S-cone function in a strongly nocturnal mammal and then investigate various aspects of circadian behavioral patterns in the animals with S-cone function restored compared to the wild-type animals. For these experiments, we chose the Syrian hamster. Previously, the UV/S-opsin gene was isolated in the Syrian hamster. The sequence for this gene was discovered to contain a single nucleotide deletion at residue 92 (GENBANK accession #AY029607), which results in a shift in the reading frame and the insertion of a premature stop codon such that if the gene were translated the truncated protein would be expected to be non-functional.[117] In the Syrian hamster, no photoreceptors could be labeled with a UV/S-opsin-specific antibody, indicating that, like human tritanopes, the S-cones in this species degenerate; however, UV opsin transcripts can be detected in the retina.[118]

What might be a nocturnal terrestrial mammal's selective advantage in losing S-cones? In primates, M1 ipRGCs have S-OFF light responses, which means they are excited by the onset of long-wavelength lights in the green-yellow-red part of the spectrum. M2 ipRGCs have S-ON light responses and are excited by the onset of short wavelength lights in the violet-blue part of the spectrum. What both types of ipRGCs have in common is that they do not respond well to white light, which contains both short and long wavelengths. Nocturnal mammals have a strong aversion to light, and they prefer to stay in the dark.[119] It has been shown that ipRGC influence mood via distinct output streams.[1] I hypothesize that ipRGCs are responsible for animals' emotional response to light including fear, anxiety and aversion that nocturnal animals experience and that activation of the ipRGCs triggers an aversive response. Nocturnal mammals have adopted a lifestyle that allows them to avoid detection by potential predators that hunt during the day; thus, avoiding going outside their burrows in the daytime protects them from predation.[120] However, the S vs. M/L color opponency observed in diurnal animals[8,67,116] renders the ipRGCs relatively insensitive to white light like during the day. Thus, a nocturnal mammal with S vs. M/L opponent ipRGCs could unwittingly wander outside because of failing to receive the appropriate danger signals and fall victim to predation. By losing the S-cones and the opponent signals in ipRGCs that prevent their activation by white light, the ipRGCs become sensitive to all lights that are absorbed by their middle-to-long wavelength cones. Activation of the ipRGCs may also suppress alertness in nocturnal animals promoting sleep during the day when it is light outside. My hypothesis predicts that correcting the S-cone gene mutation will cause the hamsters to lose their aversion to white light and cause them to be more active during the light phase of their day.

4.2 Methods

4.2.1 *Animals and sequencing of the Opn1sw gene*

All experiments were performed with approval from the University of Washington Institutional Animal Care and Use Committee. This study included four Syrian Golden Hamsters (*Mesocricetus auratus*) in which a germ-line nucleotide insertion in codon 88 of the *Opn1sw* gene was made using Crispr/Cas9 gene editing[121] by the Utah State University transgenic hamster core facility. The gene edit was meant to reverse a species-wide nucleotide deletion thought to be responsible for the absence of functional S-cones in this species. The nucleotide insert resulted in codon 88 specifying a threonine residue, which is what is found in the S-opsin gene in humans, mice, and Siberian Hamsters (a hamster species with functional S cones).

We confirmed the gene edit by sequencing the *Opn1sw* gene of the four founder animals we received. We also sequenced the exons and intron/exon junctions of the *Opn1sw* gene in the gene-modified hamsters. The *M. auratus* edited *Opn1sw* gene is 3,554 nucleotides in length from the ATG translation start codon to the TAA translation termination codon. Primers for amplification and sequencing of the gene were designed using the Geneious computer program and using the *M. Auratus Opn1sw* reference sequence. Polymerase chain reaction (PCR) amplifications were performed using Platinum Taq HiFi (Thermofisher) following the manufacturers recommendations. PCR products were prepared for Sanger Sequencing using the Edge Biosystems Quickstep 2 Purification kit following the kit instructions. Sequencing was performed using the Applied Biosystems BigDye Terminator V3.1 kit, cleaned up with the Xterminator reagent, and run on an ABI 3500XL instrument.

4.2.2 *Mating*

Founder males and females were bred, and the Opn1sw gene in offspring and founders was sequenced. The founders were homozygous for the desired gene edit but heterozygous at four other positions in the Opn1sw gene. Of the offspring, 1 male was homozygous for the allele that matched the reference sequence most closely. Two female offspring were heterozygous for the two Opn1sw alleles, none were homozygous for the sequence that most closely matched the reference (heretofore referred to as the correct allele). The homozygous male was mated to the two heterozygous females, and the offspring were genotyped. Genotyping was performed using fresh stool samples (hamsters are individually housed) with the Qiagen fast stool DNA isolation kit.

4.2.3 *Messenger RNA analysis*

Messenger RNA (mRNA) was isolated from retinas of heterozygous animals using the Takara Nucleospin RNA plus kit. mRNA was reverse transcribed using the Takara Prime Star kit, PCR amplified with Platinum Taq HiFi, and the cDNA was cloned and sequenced. The splicing isoforms obtained were aligned to the reference sequence using Geneious software, and were analyzed for the presence of cryptic splice sites using Crypt-skip (https://cryp-skip.img.cas.cz/).

4.2.4 *Euthanasia*

Animals were euthanized by an overdose of Beuthanasia-D administered intraperitoneally according to IACUC and USDA protocols. Eyes were enucleated, and retinas were either isolated for nucleic acid analyses, or fixed in 4% paraformaldehyde and dissected for immunohistochemistry (IHC).

4.2.5 *Immunohistochemistry*

For IHC, flat-mounts or 20 µm cryosections were blocked (5% normal donkey serum, 1 mg/mL bovine serum albumin, 1% Triton X-100 in PBS, pH 7.4), then incubated overnight in primary antibodies (see Table 4.3) with rhodamine-conjugated peanut agglutinin (PNA, Vector Labs RL-1072, 1:1,000). After washing, samples were incubated 2 h in secondary antibodies with DAPI counterstain (1:1,000), then mounted with Vectashield. Fluorescence was imaged using a Leica SP8 confocal with 20X or 63X oil objectives, and images were processed using ImageJ. Presented images are maximum intensity Z-projections unless noted. Retinal cryosections from wild-type C57BL/6J mice were included as controls for S-opsin antibodies.

Table 4.3 Antibodies used for IHC

	Target	Host	Catalog #	Dilution	Conjugate
1•	S opsin (mouse N terminus)	goat	Rockland 600-101-MP7	1:200	
	S opsin (mouse internal)	goat	Santa Cruz sc14365	1:100	
	S opsin (human C terminus)	rabbit	JH455 (from J. Nathans, see PMID 1524826)	1:5,000	
	S opsin (human recombinant)	rabbit	Millipore AB5407	1:5,000	
	L/M opsin (human recombinant)	rabbit	Millipore AB5405	1:200	
	MTCO1 (mitochondrial complex IV)	mouse	Abcam ab14705	1:500	
2•	Rabbit IgG	goat	A-21072	1:500	AlexaFluor633
	Goat IgG	donkey	A-21082	1:500	AlexaFluor633
	Mouse IgG	donkey	A-21202	1:500	AlexaFluor488

4.3 RESULTS

4.3.1 *Opn1sw gene sequence in the gene edited hamsters*

Sequence analysis revealed that the founder hamsters were homozygous for the desired gene edit in codon 88 of the *Opn1sw* gene, but were heterozygous at four other locations. Table 4.4 shows the differences. There was a missense mutation in exon 2 in codon 164. The correct allele specified Alanine as does the reference sequence. However, in the human (NCBI ID 611) and mouse (NCBI ID 12057) *Opn1sw* genes this codon specifies proline. There is a silent nucleotide change at the 5' end of exon 4. At this location, the correct allele does not match the reference sequence, but the other allele does. In intron 4, there is a polymorphism in the third position of intron 4. The correct allele matches the reference at this site, and this is also what is present in the human and mouse *Opn1sw* genes. Finally, there is a silent mutation in exon 5 of the gene, and the correct allele matches the reference at this position. Thus, in all, the correct allele (number 5 in Table 4.4) matches the reference sequence at 3 of the 4 variant nucleotide positions.

Table 4.4. Nucleotide differences between *Opn1sw* alleles in the gene-edited Hamsters

Nucleotide # and location[1]	Hamster 5[2]	Hamster 11[2]	Notes
264 (exon 1, codon 88)	C	C	Crispr introduced insertion to create codon 88 = Thr
493 (exon 2)	**<u>G</u>**	A	Missense GCA = Ala (annotated has Ala), ACA =Thr mutation
685 (exon 4, 5'end)	A	**<u>G</u>**	Silent (GTA/GTG, but could affect splicing); genome has GTG
921 + 3 (intron 4)	**<u>A</u>**	T	Ham 5 has what human has, change in 11 could affect splicing
975 (exon 5)	**<u>C</u>**	T	Silent

[1]Nucleotide numbers are relative to the ATG translation start codon in the cDNA.

[2]Bold, underlined nucleotides match the M. auratus consensus Opn1sw reference sequence (NCBI 101836432)

4.3.2 *Analysis of retinal mRNA from gene-edited hamsters*

Forty-eight *Opn1sw* cDNA clones obtained from heterozygous hamsters were sequenced. Only the correct allele gave rise to full-length mRNA (data not shown). The other allele gave multiple splicing isoforms that could not encode a functional S-opsin. mRNA from three animals homozygous for the correct allele was also isolated. The mRNA was reverse transcribed, and PCR amplified. The absence of contaminating gDNA was confirmed by including PCR reactions with reverse transcriptase (RT) reactions with and without the RT enzyme (see Figure 4.1). Running the gel further revealed two distinct bands, one corresponding in length to the expected full-length mRNA, and a shorter transcript. The PCR products were used in Sanger Sequencing. Sequencing results for the two splicing isoforms are shown in Figure 4.3. The shorter mRNA had a deletion of the last 189 nucleotides of exon 4. There was an apparent cryptic splice site within exon 4 that was used to splice the first 51 nucleotides of exon 4 to exon 5.

The sequences of intron 3, exon 4, intron 4, and exon 5 of the correct and incorrect alleles of the gene-edited hamster *Opn1sw* gene were analyzed with Crypt-Skip. Both alleles gave the same results (see Figure 4.3; only the good allele is shown). There is predicted to be a 47% chance of a cryptic splice site in exon 4. The cryptic splice site with a 38% score is the one that we observe in the mRNA.

1 2 3 4 5 6 7 8 9

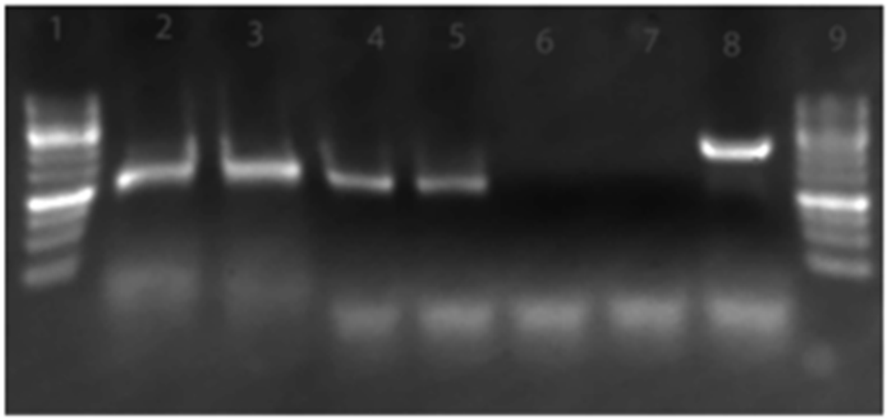

Figure 4.1 Lanes 1-9 from right to left

1kb ladder

Hamster #25 5μL of RT amplified with Takara PrimeStar

Hamster #33 5μL of RT amplified with Takara PrimeStar

Hamster #25 5μL of RT amplified with HiFi Taq

Hamster #33 5μL of RT amplified with HiFi Taq

Hamster #25 5μL of RT without RT amplified with HiFi Taq

Hamster #33 5μL of RT without RT amplified with HiFi Taq

Hamster gDNA 1μL amplified with HiFi enzyme (DNA control)

1kb ladder

To summarize the DNA results, the wild-type coding sequence for *Opn1sw* was restored in one allele (except for one silent nucleotide substitution that did not match the reference sequence) in a line of CRISPR-corrected hamsters (Figure 4.3). A line of animals homozygous for the correct allele was bred. Genomic DNA and mRNA for corrected *Opn1sw* was found in CRISPR-corrected hamster retinas. The retinas of animals that were homozygous for the corrected allele were the subject of immunostaining to look for corrected S-cones.

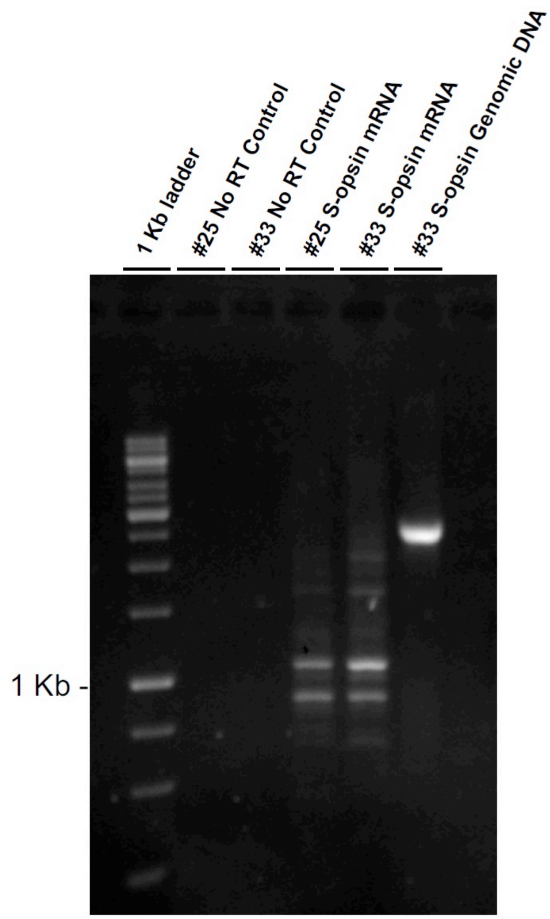

Figure 4.2 Corrected gDNA was detected in retinal homogenates from two CRISPR corrected hamsters (right panel, far right lane). Multiple splice variants encoding corrected Opn1sw were found in cDNA generated from mRNA transcript

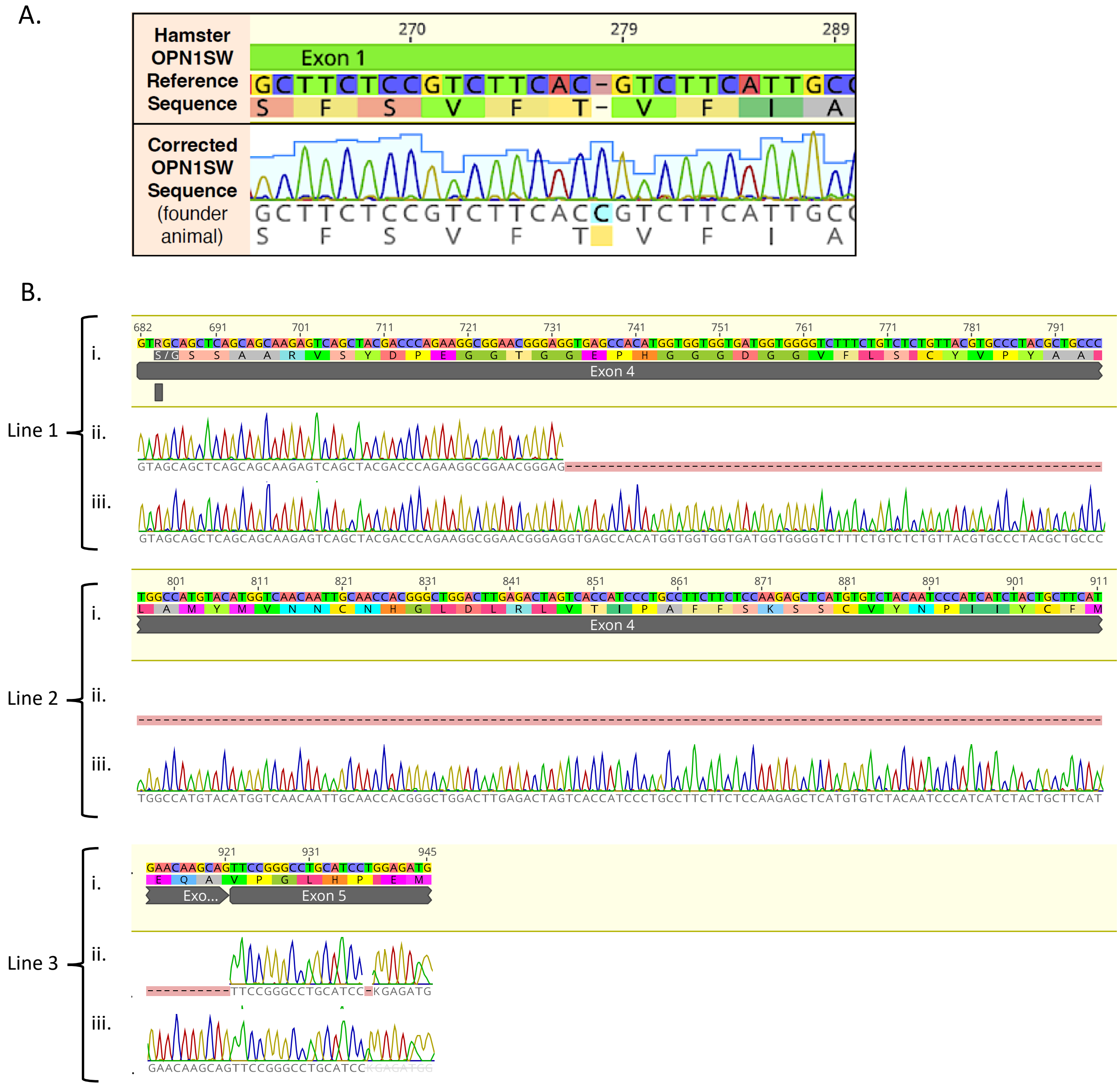

Figure 4.3 Sequencing data confirmed that the coding sequence had been corrected in CRISPR-corrected animals and the short mRNA product is the result of exon skipping in exon 4. A.) CRISPR successfully inserted a nucleotide (blue) in Codon 88 in the founder hamster. B.) Three lines of sequencing data for ii.) the short mRNA product and iii.) the full-length mRNA product are compared against i.) the reference sequence. The short mRNA product splices part of exon 4 (line 1) to exon 5 (line 3).

4.3.3 *Immunostaining of S-opsin*

Immunostaining for S-opsin in retinal cryosections from two CRISPR corrected hamsters is shown in Figure 4.4. Immunolabeling results for the hamsters were compared with those from wild-type mice. Cone sheaths were labeled with PNA (magenta), and four different antibodies directed against S-opsin were used just in case hamster S-opsin was present but did not cross-react with a particular antibody. All four antibodies reacted with mouse cone outer segments. However, none of the hamster cones labeled with PNA cross-reacted with any of the antibodies. There are a few things to consider here. First, being strongly nocturnal, the hamsters have very few cones. Thus, only a few cones are seen in any one cryosection. Second, mice are very unusual among all mammals in that most cones in the inferior retina express short wavelength sensitive (UV) photopigment. For most mammals, only 5-10% of cones express S-opsin. Thus, it might be possible, given the small number of cones present in each cryosection and the expected scarcity of S-cones even in the corrected hamster retina, that the S-cones are being missed. Therefore, we did immunochemistry in retinal flat mounts, allowing many more cones to be examined.

Immunostaining of S- or M-opsin in the outer segment layer of retinal flat-mounts from three CRISPR corrected hamsters is shown in Figure 4.5. Cone outer segments were labeled with PNA (magenta), and opsins were labeled using antibodies directed against S- or M-opsin (green; 600-101-MP7 and AB5405, respectively). M-opsin staining shown in Figure 4.5 shows healthy cone outer segments co-localizing with the PNA-stained cone sheaths.

However, robust expression of S-opsin protein was not detected in the corrected hamster retinas using IHC with antibodies that strongly label rodent S-opsin. Animals were examined at different ages, three weeks, three months, and ten months, in case S-cones develop early in life but degenerate later. There were no obvious differences between the different ages.

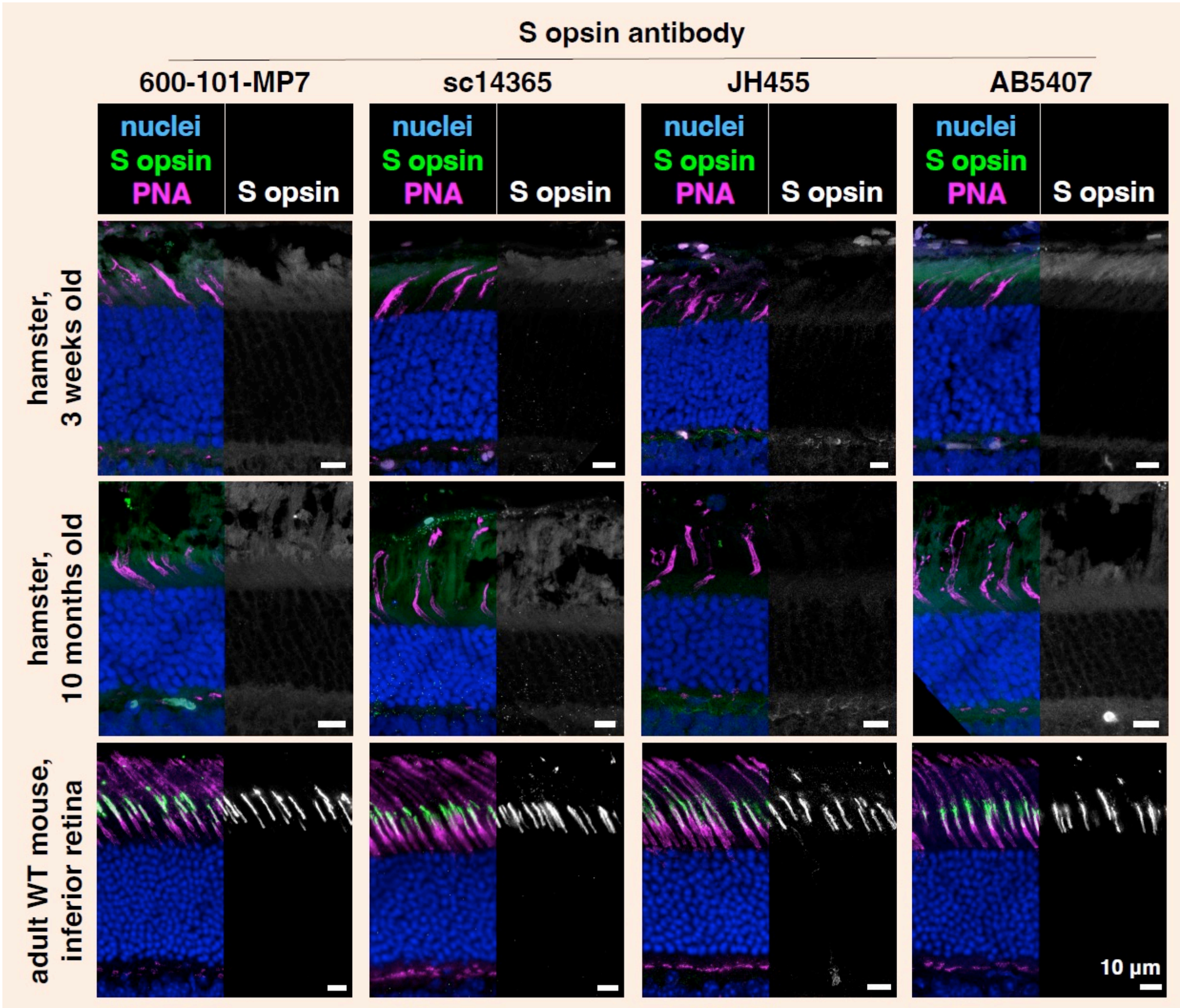

Figure 4.4 Immunostaining of S-opsin in retinal cryosections from two CRISPR corrected hamsters (top, middle) and wild-type mouse (bottom). Cone outer segments were labelled with PNA (magenta) and S-opsin was labelled using one of four antibodies directed against S-opsin (green). Robust expression of S-opsin was not detected in the corrected hamster retinas.

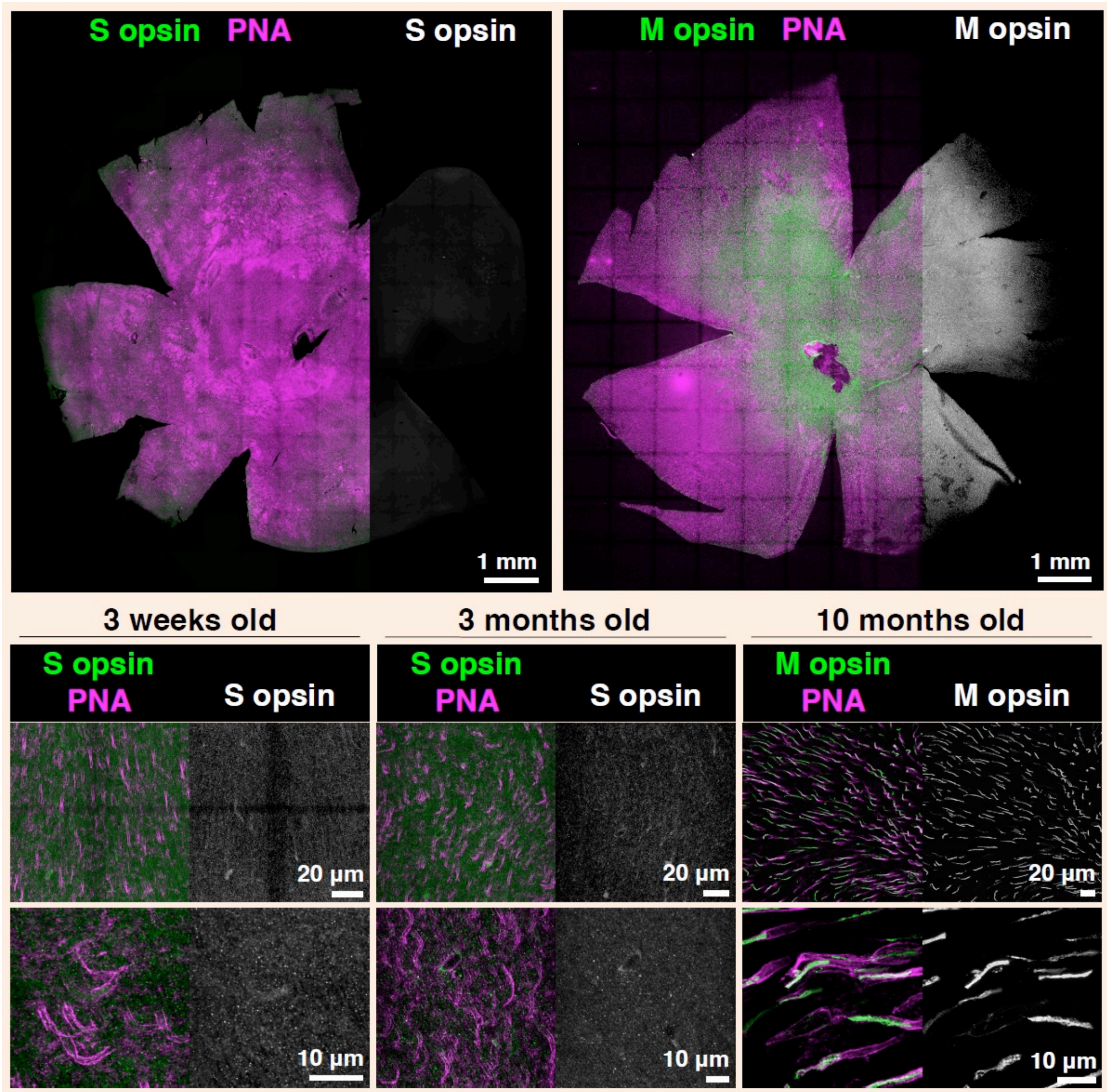

Figure 4.5 Immunostaining of S- or M-opsin in the outer segment layer of retinal flatmounts from three CRISPR corrected hamsters. Cone outer segments were labelled with PNA (magenta) and opsins were labelled using antibodies directed agains S- or M-opsin (green; 600-101-MP7 and AB5405, respectively).

However, on close examination, as shown in Figure 4.6**,** a population of cones across the retina was found to have rounded, abnormal-appearing outer segments containing mislocalized nuclei and a faint S-opsin signal. Mitochondria, normally abundant in the cone ellipsoid region, were also mis-localized in the outer segment layer. Around 45 cones are visible by PNA staining in the left panel of Figure 4.6, and three of them, or about 6-7%, exhibit the pattern of abnormal appearance and faint S-opsin staining near the distal end of the cell. This number is consistent with the number of S-cones in most mammals, including humans. One cone, shown in Figure 4.6 (lower right inset), showed a better-developed outer segment, but it also exhibited the odd morphology where the nucleus was misplaced.

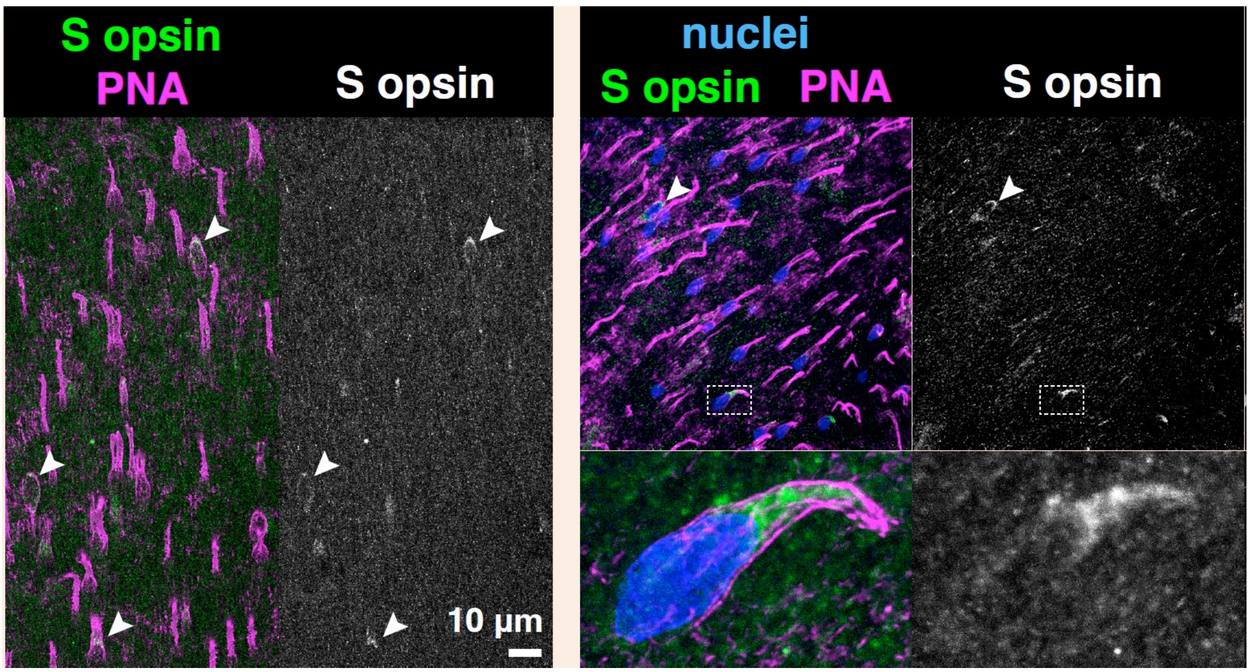

Figure 4.6 Immunostaining showing abnormal cone outer segments with weak S-opsin expression and distally mislocalized nuclei in flat mounts (top, arrowheads and inset).

4.4 Discussion

I predicted that repairing the single base-pair deletion in the hamster would restore S-cone function like I imagine an ancient ancestor would have before hamsters evolved retinas without S-cones. However, S-cone morphology was only very fractionally restored. The faint staining indicates that only a very small amount of S-cone opsin is produced, and we don't know if it is functional. In addition, the morphology of the cones is very abnormal. We tried an ERG with 360 nm light and there was no detectable response attributable to UV sensitive cones. Thus, experiments to test for a difference in circadian behavior between the wildtype and the corrected hamsters are not warranted. Insight into why so many mammals have evolved S-cone pseudogenes will have to wait until we figure out how to fully correct the S-cone defect in these animals. Multiple splice variants encoding corrected *Opn1sw* were found in cDNA that was generated from mRNA transcripts (Figure 4.2). Therefore, only a fraction of the cDNA generated gave rise to full-length *Opn1sw* mRNA. If less opsin is produced, this could result in shorter outer segments but it does not seem to fully explain the S-cone defect in the corrected animals because splicing defects and haploinsufficiency seem to be normal for S-cones in many species including humans.[122]

The fact that about 6-7% of cones weakly express S-opsin suggests that the loss of S-cones occurred in an ancestor that had a typical ratio of S-cones to M/L cones. The fact that we were unable to fully restore cone function in the hamsters suggests that the opsin may have more than one gene defect. One candidate is codon 164 where the correct allele specified alanine as does the reference sequence. However, in the human (NCBI ID 611) and mouse (NCBI ID 12057) *Opn1sw* genes, this codon specifies proline. A proline to alanine substitution seems like it could have a significant effect on function. One future step could be to change the alanine to proline and see if cone function is restored. However, that is beyond the scope of the experiments I am reporting here.

BIBLIOGRAPHY

1. Fernandez, D.C., Fogerson, P.M., Lazzerini Ospri, L., Thomsen, M.B., Layne, R.M., Severin, D., Zhan, J., Singer, J.H., Kirkwood, A., Zhao, H., et al. (2018). Light Affects Mood and Learning through Distinct Retina-Brain Pathways. Cell *175*, 71-84 e18. 10.1016/j.cell.2018.08.004.
2. Hattar, S., Liao, H.W., Takao, M., Berson, D.M., and Yau, K.W. (2002). Melanopsin-containing retinal ganglion cells: architecture, projections, and intrinsic photosensitivity. Science *295*, 1065-1070. 10.1126/science.1069609.
3. Freedman, M.S., Lucas, R.J., Soni, B., von Schantz, M., Munoz, M., David-Gray, Z., and Foster, R. (1999). Regulation of mammalian circadian behavior by non-rod, non-cone, ocular photoreceptors. Science *284*, 502-504. 10.1126/science.284.5413.502.
4. Panda, S., Provencio, I., Tu, D.C., Pires, S.S., Rollag, M.D., Castrucci, A.M., Pletcher, M.T., Sato, T.K., Wiltshire, T., Andahazy, M., et al. (2003). Melanopsin is required for non-image-forming photic responses in blind mice. Science *301*, 525-527. 10.1126/science.1086179.
5. van Diepen, H.C., Schoonderwoerd, R.A., Ramkisoensing, A., Janse, J.A.M., Hattar, S., and Meijer, J.H. (2021). Distinct contribution of cone photoreceptor subtypes to the mammalian biological clock. Proc Natl Acad Sci U S A *118*. 10.1073/pnas.2024500118.
6. Lucas, R.J., Peirson, S.N., Berson, D.M., Brown, T.M., Cooper, H.M., Czeisler, C.A., Figueiro, M.G., Gamlin, P.D., Lockley, S.W., O'Hagan, J.B., et al. (2014). Measuring and using light in the melanopsin age. Trends Neurosci *37*, 1-9. 10.1016/j.tins.2013.10.004.
7. Dacey, D.M., Liao, H.W., Peterson, B.B., Robinson, F.R., Smith, V.C., Pokorny, J., Yau, K.W., and Gamlin, P.D. (2005). Melanopsin-expressing ganglion cells in primate retina signal colour and irradiance and project to the LGN. Nature *433*, 749-754. 10.1038/nature03387.
8. Patterson, S.S., Neitz, M., and Neitz, J. (2022). S-cone circuits in the primate retina for non-image-forming vision. Semin Cell Dev Biol *126*, 66-70. 10.1016/j.semcdb.2021.05.004.
9. Schmidt, T.M., and Kofuji, P. (2010). Differential cone pathway influence on intrinsically photosensitive retinal ganglion cell subtypes. J Neurosci *30*, 16262-16271. 10.1523/JNEUROSCI.3656-10.2010.
10. Chen, S.K., Badea, T.C., and Hattar, S. (2011). Photoentrainment and pupillary light reflex are mediated by distinct populations of ipRGCs. Nature *476*, 92-95. 10.1038/nature10206.
11. Mure, L.S., Vinberg, F., Hanneken, A., and Panda, S. (2019). Functional diversity of human intrinsically photosensitive retinal ganglion cells. Science *366*, 1251-1255. 10.1126/science.aaz0898.
12. Packer, O.S., Verweij, J., Li, P.H., Schnapf, J.L., and Dacey, D.M. (2010). Blue-yellow opponency in primate S cone photoreceptors. J Neurosci *30*, 568-572. 10.1523/JNEUROSCI.4738-09.2010.
13. Patterson, S.S., Kuchenbecker, J.A., Anderson, J.R., Neitz, M., and Neitz, J. (2020). A Color Vision Circuit for Non-Image-Forming Vision in the Primate Retina. Curr Biol *30*, 1269-1274 e1262. 10.1016/j.cub.2020.01.040.
14. Patterson, S.S., Mazzaferri, M.A., Bordt, A.S., Chang, J., Neitz, M., and Neitz, J. (2020). Another Blue-ON ganglion cell in the primate retina. Curr Biol *30*, R1409-R1410. 10.1016/j.cub.2020.10.010.
15. Gooley, J.J., Rajaratnam, S.M., Brainard, G.C., Kronauer, R.E., Czeisler, C.A., and Lockley, S.W. (2010). Spectral responses of the human circadian system depend on the irradiance and duration of exposure to light. Sci Transl Med *2*, 31ra33. 10.1126/scitranslmed.3000741.
16. Smith, M.R., Burgess, H.J., Fogg, L.F., and Eastman, C.I. (2009). Racial differences in the human endogenous circadian period. PLoS One *4*, e6014. 10.1371/journal.pone.0006014.
17. Casiraghi, L.P., Plano, S.A., Fernandez-Duque, E., Valeggia, C., Golombek, D.A., and de la Iglesia, H.O. (2020). Access to electric light is associated with delays of the dim-light melatonin onset in a traditionally hunter-gatherer Toba/Qom community. J Pineal Res *69*, e12689. 10.1111/jpi.12689.
18. Stothard, E.R., McHill, A.W., Depner, C.M., Birks, B.R., Moehlman, T.M., Ritchie, H.K., Guzzetti, J.R., Chinoy, E.D., LeBourgeois, M.K., Axelsson, J., and Wright, K.P., Jr. (2017). Circadian Entrainment to the Natural Light-Dark Cycle across Seasons and the Weekend. Curr Biol *27*, 508-513. 10.1016/j.cub.2016.12.041.
19. Wright, K.P., Jr., McHill, A.W., Birks, B.R., Griffin, B.R., Rusterholz, T., and Chinoy, E.D. (2013). Entrainment of the human circadian clock to the natural light-dark cycle. Curr Biol *23*, 1554-1558. 10.1016/j.cub.2013.06.039.

20. St Hilaire, M.A., Gooley, J.J., Khalsa, S.B., Kronauer, R.E., Czeisler, C.A., and Lockley, S.W. (2012). Human phase response curve to a 1 h pulse of bright white light. J Physiol *590*, 3035-3045. 10.1113/jphysiol.2012.227892.
21. Roenneberg, T., Pilz, L.K., Zerbini, G., and Winnebeck, E.C. (2019). Chronotype and Social Jetlag: A (Self-) Critical Review. Biology (Basel) *8*. 10.3390/biology8030054.
22. Crowley, S.J., and Carskadon, M.A. (2010). Modifications to weekend recovery sleep delay circadian phase in older adolescents. Chronobiol Int *27*, 1469-1492. 10.3109/07420528.2010.503293.
23. Burgess, H.J., and Eastman, C.I. (2006). A late wake time phase delays the human dim light melatonin rhythm. Neurosci Lett *395*, 191-195. 10.1016/j.neulet.2005.10.082.
24. St Hilaire, M.A., Amundadottir, M.L., Rahman, S.A., Rajaratnam, S.M.W., Ruger, M., Brainard, G.C., Czeisler, C.A., Andersen, M., Gooley, J.J., and Lockley, S.W. (2022). The spectral sensitivity of human circadian phase resetting and melatonin suppression to light changes dynamically with light duration. Proc Natl Acad Sci U S A *119*, e2205301119. 10.1073/pnas.2205301119.
25. Zeitzer, J.M., Ruby, N.F., Fisicaro, R.A., and Heller, H.C. (2011). Response of the human circadian system to millisecond flashes of light. PLoS One *6*, e22078. 10.1371/journal.pone.0022078.
26. Abrahamson, E.E., and Moore, R.Y. (2001). Suprachiasmatic nucleus in the mouse: retinal innervation, intrinsic organization and efferent projections. Brain Res *916*, 172-191. 10.1016/s0006-8993(01)02890-6.
27. Fernandez, D.C., Chang, Y.T., Hattar, S., and Chen, S.K. (2016). Architecture of retinal projections to the central circadian pacemaker. Proc Natl Acad Sci U S A *113*, 6047-6052. 10.1073/pnas.1523629113.
28. Jones, J.R., Chaturvedi, S., Granados-Fuentes, D., and Herzog, E.D. (2021). Circadian neurons in the paraventricular nucleus entrain and sustain daily rhythms in glucocorticoids. Nat Commun *12*, 5763. 10.1038/s41467-021-25959-9.
29. Collins, B., Pierre-Ferrer, S., Muheim, C., Lukacsovich, D., Cai, Y., Spinnler, A., Herrera, C.G., Wen, S., Winterer, J., Belle, M.D.C., et al. (2020). Circadian VIPergic Neurons of the Suprachiasmatic Nuclei Sculpt the Sleep-Wake Cycle. Neuron *108*, 486-499 e485. 10.1016/j.neuron.2020.08.001.
30. Wen, S., Ma, D., Zhao, M., Xie, L., Wu, Q., Gou, L., Zhu, C., Fan, Y., Wang, H., and Yan, J. (2020). Spatiotemporal single-cell analysis of gene expression in the mouse suprachiasmatic nucleus. Nat Neurosci *23*, 456-467. 10.1038/s41593-020-0586-x.
31. Kim, K.Y., Rios, L.C., Le, H., Perez, A.J., Phan, S., Bushong, E.A., Deerinck, T.J., Liu, Y.H., Ellisman, M.A., Lev-Ram, V., et al. (2019). Synaptic Specializations of Melanopsin-Retinal Ganglion Cells in Multiple Brain Regions Revealed by Genetic Label for Light and Electron Microscopy. Cell Rep *29*, 628-644 e626. 10.1016/j.celrep.2019.09.006.
32. Mazuski, C., Chen, S.P., and Herzog, E.D. (2020). Different Roles for VIP Neurons in the Neonatal and Adult Suprachiasmatic Nucleus. J Biol Rhythms *35*, 465-475. 10.1177/0748730420932073.
33. Welsh, D.K., Yoo, S.H., Liu, A.C., Takahashi, J.S., and Kay, S.A. (2004). Bioluminescence imaging of individual fibroblasts reveals persistent, independently phased circadian rhythms of clock gene expression. Curr Biol *14*, 2289-2295. 10.1016/j.cub.2004.11.057.
34. Liu, A.C., Welsh, D.K., Ko, C.H., Tran, H.G., Zhang, E.E., Priest, A.A., Buhr, E.D., Singer, O., Meeker, K., Verma, I.M., et al. (2007). Intercellular coupling confers robustness against mutations in the SCN circadian clock network. Cell *129*, 605-616. 10.1016/j.cell.2007.02.047.
35. Yamaguchi, S., Isejima, H., Matsuo, T., Okura, R., Yagita, K., Kobayashi, M., and Okamura, H. (2003). Synchronization of cellular clocks in the suprachiasmatic nucleus. Science *302*, 1408-1412. 10.1126/science.1089287.
36. Liu, C., and Reppert, S.M. (2000). GABA synchronizes clock cells within the suprachiasmatic circadian clock. Neuron *25*, 123-128. 10.1016/s0896-6273(00)80876-4.
37. Aton, S.J., Huettner, J.E., Straume, M., and Herzog, E.D. (2006). GABA and Gi/o differentially control circadian rhythms and synchrony in clock neurons. Proc Natl Acad Sci U S A *103*, 19188-19193. 10.1073/pnas.0607466103.
38. Evans, J.A., Leise, T.L., Castanon-Cervantes, O., and Davidson, A.J. (2013). Dynamic interactions mediated by nonredundant signaling mechanisms couple circadian clock neurons. Neuron *80*, 973-983. 10.1016/j.neuron.2013.08.022.
39. Todd, W.D., Venner, A., Anaclet, C., Broadhurst, R.Y., De Luca, R., Bandaru, S.S., Issokson, L., Hablitz, L.M., Cravetchi, O., Arrigoni, E., et al. (2020). Suprachiasmatic VIP neurons are required for normal circadian rhythmicity and comprised of molecularly distinct subpopulations. Nat Commun *11*, 4410. 10.1038/s41467-020-17197-2.

40. Maejima, T., Tsuno, Y., Miyazaki, S., Tsuneoka, Y., Hasegawa, E., Islam, M.T., Enoki, R., Nakamura, T.J., and Mieda, M. (2021). GABA from vasopressin neurons regulates the time at which suprachiasmatic nucleus molecular clocks enable circadian behavior. Proc Natl Acad Sci U S A *118*. 10.1073/pnas.2010168118.
41. Maywood, E.S., Chesham, J.E., O'Brien, J.A., and Hastings, M.H. (2011). A diversity of paracrine signals sustains molecular circadian cycling in suprachiasmatic nucleus circuits. Proc Natl Acad Sci U S A *108*, 14306-14311. 10.1073/pnas.1101767108.
42. Colwell, C.S., Michel, S., Itri, J., Rodriguez, W., Tam, J., Lelievre, V., Hu, Z., Liu, X., and Waschek, J.A. (2003). Disrupted circadian rhythms in VIP- and PHI-deficient mice. Am J Physiol Regul Integr Comp Physiol *285*, R939-949. 10.1152/ajpregu.00200.2003.
43. Harmar, A.J., Marston, H.M., Shen, S., Spratt, C., West, K.M., Sheward, W.J., Morrison, C.F., Dorin, J.R., Piggins, H.D., Reubi, J.C., et al. (2002). The VPAC(2) receptor is essential for circadian function in the mouse suprachiasmatic nuclei. Cell *109*, 497-508. 10.1016/s0092-8674(02)00736-5.
44. Brown, T.M., Colwell, C.S., Waschek, J.A., and Piggins, H.D. (2007). Disrupted neuronal activity rhythms in the suprachiasmatic nuclei of vasoactive intestinal polypeptide-deficient mice. J Neurophysiol *97*, 2553-2558. 10.1152/jn.01206.2006.
45. Hughes, A.T., Guilding, C., Lennox, L., Samuels, R.E., McMahon, D.G., and Piggins, H.D. (2008). Live imaging of altered period1 expression in the suprachiasmatic nuclei of Vipr2-/- mice. J Neurochem *106*, 1646-1657. 10.1111/j.1471-4159.2008.05520.x.
46. Aton, S.J., Colwell, C.S., Harmar, A.J., Waschek, J., and Herzog, E.D. (2005). Vasoactive intestinal polypeptide mediates circadian rhythmicity and synchrony in mammalian clock neurons. Nat Neurosci *8*, 476-483. 10.1038/nn1419.
47. Yamaguchi, Y., Suzuki, T., Mizoro, Y., Kori, H., Okada, K., Chen, Y., Fustin, J.M., Yamazaki, F., Mizuguchi, N., Zhang, J., et al. (2013). Mice genetically deficient in vasopressin V1a and V1b receptors are resistant to jet lag. Science *342*, 85-90. 10.1126/science.1238599.
48. Golombek, D.A., and Rosenstein, R.E. (2010). Physiology of circadian entrainment. Physiol Rev *90*, 1063-1102. 10.1152/physrev.00009.2009.
49. Jones, J.R., Simon, T., Lones, L., and Herzog, E.D. (2018). SCN VIP Neurons Are Essential for Normal Light-Mediated Resetting of the Circadian System. J Neurosci *38*, 7986-7995. 10.1523/JNEUROSCI.1322-18.2018.
50. Abel, J.H., Meeker, K., Granados-Fuentes, D., St John, P.C., Wang, T.J., Bales, B.B., Doyle, F.J., 3rd, Herzog, E.D., and Petzold, L.R. (2016). Functional network inference of the suprachiasmatic nucleus. Proc Natl Acad Sci U S A *113*, 4512-4517. 10.1073/pnas.1521178113.
51. Pennartz, C.M., Hamstra, R., and Geurtsen, A.M. (2001). Enhanced NMDA receptor activity in retinal inputs to the rat suprachiasmatic nucleus during the subjective night. J Physiol *532*, 181-194. 10.1111/j.1469-7793.2001.0181g.x.
52. Colwell, C.S. (2001). NMDA-evoked calcium transients and currents in the suprachiasmatic nucleus: gating by the circadian system. Eur J Neurosci *13*, 1420-1428. 10.1046/j.0953-816x.2001.01517.x.
53. Girardet, C., Blanchard, M.P., Ferracci, G., Leveque, C., Moreno, M., Francois-Bellan, A.M., Becquet, D., and Bosler, O. (2010). Daily changes in synaptic innervation of VIP neurons in the rat suprachiasmatic nucleus: contribution of glutamatergic afferents. Eur J Neurosci *31*, 359-370. 10.1111/j.1460-9568.2009.07071.x.
54. Panda, S., Antoch, M.P., Miller, B.H., Su, A.I., Schook, A.B., Straume, M., Schultz, P.G., Kay, S.A., Takahashi, J.S., and Hogenesch, J.B. (2002). Coordinated transcription of key pathways in the mouse by the circadian clock. Cell *109*, 307-320. 10.1016/s0092-8674(02)00722-5.
55. Becquet, D., Girardet, C., Guillaumond, F., Francois-Bellan, A.M., and Bosler, O. (2008). Ultrastructural plasticity in the rat suprachiasmatic nucleus. Possible involvement in clock entrainment. Glia *56*, 294-305. 10.1002/glia.20613.
56. Khalsa, S.B., Jewett, M.E., Cajochen, C., and Czeisler, C.A. (2003). A phase response curve to single bright light pulses in human subjects. Journal of Physiology *549*, 945-952.
57. Figueiro, M.G., Bullough, J.D., Parsons, R.H., and Rea, M.S. (2004). Preliminary evidence for spectral opponency in the suppression of melatonin by light in humans. Neuroreport *15*, 313-316.
58. Brown, T.M., Thapan, K., Arendt, J., Revell, V.L., and Skene, D.J. (2021). S-cone contribution to the acute melatonin suppression response in humans. Journal of pineal research *71*, e12719.
59. Neitz, J., Carroll, J., Yamauchi, Y., Neitz, M., and Williams, D.R. (2002). Color perception in mediated by a plastic neural mechanism that is adjustable in adults. Neuron *35*, 783-792.

60. Carroll, J., McMahon, C., Neitz, M., and Neitz, J. (2000). Flicker-photometric electroretinogram estimates of L : M cone photoreceptor ratio in men with photopigment spectra derived from genetics. JOSAA *17*, 499-509.
61. Van De Kraats, J., and Van Norren, D. (2007). Optical density of the aging human ocular media in the visible and the UV. JOSA A *24*, 1842-1857.
62. Hardeland, R. (2012). Neurobiology, pathophysiology, and treatment of melatonin deficiency and dysfunction. The Scientific World Journal *2012*.
63. Benloucif, S., Guico, M., Reid, K.J., Wolfe, L., L'Hermite-Balériaux, M., and Zee, P. (2005). Stability of melatonin and temperature as circadian phase markers and their relation to sleep times in humans. Journal of biological rhythms *20*, 178-188.
64. Brainard, G.C., Hanifin, J.P., Greeson, J.M., Byrne, B., Glickman, G., Gerner, E., and Rollag, M.D. (2001). Action spectrum for melatonin regulation in humans: evidence for a novel circadian photoreceptor. Journal of Neuroscience *21*, 6405-6412.
65. Thapan, K., Arendt, J., and Skene, D.J. (2001). An action spectrum for melatonin suppression: evidence for a novel non-rod, non-cone photoreceptor system in humans. Journal of Physiology *535*, 261-267.
66. Spitschan, M., Lazar, R., Yetik, E., and Cajochen, C. (2019). No evidence for an S cone contribution to acute neuroendocrine and alerting responses to light. Current Biology *29*, R1297-R1298.
67. Pauers, M., Kuchenbecker, J., Neitz, M., and J, N. (2012). Changes in the colour of light cue circadian activity. Animal Behavior *83*, 1143-1151.
68. Su, C., Luo, D., Terakita, A., Shichida, Y., Liao, H., Kazmi, M., Sakmar, T., and Yau, K.W. (2006). Parietal-eye phototransduction components and their potential evolutionary implications. Science *311*, 1617-1627.
69. Spudich, J., and Spudich, E. (2008). The simplest eyes: rhodopsin-mediated phototaxis reception in microorganisms. In Animal Models in Eye Research, P. Tsonis, ed. (Elsevier).
70. Neitz, J., and Neitz, M. (2011). The Genetics of Normal and Defective Color Vision. Vision Research *51*, 633-651.
71. Stabio, M.E., Sabbah, S., Quattrochi, L.E., Ilardi, M.C., Fogerson, P.M., Leyrer, M.L., Kim, M.T., Kim, I., Schiel, M., Renna, J.M., et al. (2018). The M5 Cell: A Color-Opponent Intrinsically Photosensitive Retinal Ganglion Cell. Neuron *97*, 150-163.e154. 10.1016/j.neuron.2017.11.030.
72. Estevez, M.E., Fogerson, P.M., Ilardi, M.C., Borghuis, B.G., Chan, E., Weng, S., Auferkorte, O.N., Demb, J.B., and Berson, D.M. (2012). Form and function of the M4 cell, an intrinsically photosensitive retinal ganglion cell type contributing to geniculocortical vision. Journal of Neuroscience *32*, 13608-13620.
73. Hastings, M.H., Maywood, E.S., and Brancaccio, M. (2018). Generation of circadian rhythms in the suprachiasmatic nucleus. Nat Rev Neurosci *19*, 453-469. 10.1038/s41583-018-0026-z.
74. Colwell, C.S. (2011). Linking neural activity and molecular oscillations in the SCN. Nat Rev Neurosci *12*, 553-569. 10.1038/nrn3086.
75. Webb, A.B., Angelo, N., Huettner, J.E., and Herzog, E.D. (2009). Intrinsic, nondeterministic circadian rhythm generation in identified mammalian neurons. Proc Natl Acad Sci U S A *106*, 16493-16498. 10.1073/pnas.0902768106.
76. Hughes, S., Jagannath, A., Hankins, M.W., Foster, R.G., and Peirson, S.N. (2015). Photic regulation of clock systems. Methods Enzymol *552*, 125-143. 10.1016/bs.mie.2014.10.018.
77. Gizowski, C., Zaelzer, C., and Bourque, C.W. (2016). Clock-driven vasopressin neurotransmission mediates anticipatory thirst prior to sleep. Nature *537*, 685-688. 10.1038/nature19756.
78. Mohawk, J.A., Green, C.B., and Takahashi, J.S. (2012). Central and peripheral circadian clocks in mammals. Annu Rev Neurosci *35*, 445-462. 10.1146/annurev-neuro-060909-153128.
79. Silver, R., LeSauter, J., Tresco, P.A., and Lehman, M.N. (1996). A diffusible coupling signal from the transplanted suprachiasmatic nucleus controlling circadian locomotor rhythms. Nature *382*, 810-813. 10.1038/382810a0.
80. Lee, I.T., Chang, A.S., Manandhar, M., Shan, Y., Fan, J., Izumo, M., Ikeda, Y., Motoike, T., Dixon, S., Seinfeld, J.E., et al. (2015). Neuromedin s-producing neurons act as essential pacemakers in the suprachiasmatic nucleus to couple clock neurons and dictate circadian rhythms. Neuron *85*, 1086-1102. 10.1016/j.neuron.2015.02.006.
81. Hughes, A.T., Fahey, B., Cutler, D.J., Coogan, A.N., and Piggins, H.D. (2004). Aberrant gating of photic input to the suprachiasmatic circadian pacemaker of mice lacking the VPAC2 receptor. J Neurosci *24*, 3522-3526. 10.1523/JNEUROSCI.5345-03.2004.

82. Vosko, A., van Diepen, H.C., Kuljis, D., Chiu, A.M., Heyer, D., Terra, H., Carpenter, E., Michel, S., Meijer, J.H., and Colwell, C.S. (2015). Role of vasoactive intestinal peptide in the light input to the circadian system. Eur J Neurosci *42*, 1839-1848. 10.1111/ejn.12919.
83. Okamoto, S., Okamura, H., Miyake, M., Takahashi, Y., Takagi, S., Akagi, Y., Fukui, K., Okamoto, H., and Ibata, Y. (1991). A diurnal variation of vasoactive intestinal peptide (VIP) mRNA under a daily light-dark cycle in the rat suprachiasmatic nucleus. Histochemistry *95*, 525-528. 10.1007/BF00315750.
84. Yang, J., Cagampang, F.R., Nakayama, Y., and Inouye, S.I. (1993). Vasoactive intestinal polypeptide precursor mRNA exhibits diurnal variation in the rat suprachiasmatic nuclei. Brain Res Mol Brain Res *20*, 259-262. 10.1016/0169-328x(93)90049-u.
85. Zoeller, R.T., Broyles, B., Earley, J., Anderson, E.R., and Alberst, H.E. (1992). Cellular levels of messenger ribonucleic acids encoding vasoactive intestinal Peptide and gastrin-releasing Peptide in neurons of the suprachiasmatic nucleus exhibit distinct 24-hour rhythms. J Neuroendocrinol *4*, 119-124. 10.1111/j.1365-2826.1992.tb00354.x.
86. Dardente, H., Menet, J.S., Challet, E., Tournier, B.B., Pevet, P., and Masson-Pevet, M. (2004). Daily and circadian expression of neuropeptides in the suprachiasmatic nuclei of nocturnal and diurnal rodents. Brain Res Mol Brain Res *124*, 143-151. 10.1016/j.molbrainres.2004.01.010.
87. Shinohara, K., Honma, S., Katsuno, Y., Abe, H., and Honma, K. (1994). Circadian rhythms in the release of vasoactive intestinal polypeptide and arginine-vasopressin in organotypic slice culture of rat suprachiasmatic nucleus. Neurosci Lett *170*, 183-186. 10.1016/0304-3940(94)90269-0.
88. Takahashi, Y., Okamura, H., Yanaihara, N., Hamada, S., Fujita, S., and Ibata, Y. (1989). Vasoactive intestinal peptide immunoreactive neurons in the rat suprachiasmatic nucleus demonstrate diurnal variation. Brain Res *497*, 374-377. 10.1016/0006-8993(89)90283-7.
89. Fernandez, M.P., Berni, J., and Ceriani, M.F. (2008). Circadian remodeling of neuronal circuits involved in rhythmic behavior. PLoS Biol *6*, e69. 10.1371/journal.pbio.0060069.
90. Depetris-Chauvin, A., Fernandez-Gamba, A., Gorostiza, E.A., Herrero, A., Castano, E.M., and Ceriani, M.F. (2014). Mmp1 processing of the PDF neuropeptide regulates circadian structural plasticity of pacemaker neurons. PLoS Genet *10*, e1004700. 10.1371/journal.pgen.1004700.
91. Herrero, A., Duhart, J.M., and Ceriani, M.F. (2017). Neuronal and Glial Clocks Underlying Structural Remodeling of Pacemaker Neurons in Drosophila. Front Physiol *8*, 918. 10.3389/fphys.2017.00918.
92. Herrero, A., Yoshii, T., Ispizua, J.I., Colque, C., Veenstra, J.A., Muraro, N.I., and Ceriani, M.F. (2020). Coupling Neuropeptide Levels to Structural Plasticity in Drosophila Clock Neurons. Curr Biol *30*, 3154-3166 e3154. 10.1016/j.cub.2020.06.009.
93. Petsakou, A., Sapsis, T.P., and Blau, J. (2015). Circadian Rhythms in Rho1 Activity Regulate Neuronal Plasticity and Network Hierarchy. Cell *162*, 823-835. 10.1016/j.cell.2015.07.010.
94. Sivachenko, A., Li, Y., Abruzzi, K.C., and Rosbash, M. (2013). The transcription factor Mef2 links the Drosophila core clock to Fas2, neuronal morphology, and circadian behavior. Neuron *79*, 281-292. 10.1016/j.neuron.2013.05.015.
95. Gunawardhana, K.L., and Hardin, P.E. (2017). VRILLE Controls PDF Neuropeptide Accumulation and Arborization Rhythms in Small Ventrolateral Neurons to Drive Rhythmic Behavior in Drosophila. Curr Biol *27*, 3442-3453 e3444. 10.1016/j.cub.2017.10.010.
96. Gundermann, D.G., Lymer, S., and Blau, J. (2023). A rapid and dynamic role for FMRP in the plasticity of adult neurons. bioRxiv. 10.1101/2023.09.01.555985.
97. Nian, X., Chen, W., Bai, W., Zhao, Z., and Zhang, Y. (2019). miR-263b Controls Circadian Behavior and the Structural Plasticity of Pacemaker Neurons by Regulating the LIM-Only Protein Beadex. Cells *8*. 10.3390/cells8080923.
98. Polcownuk, S., Yoshii, T., and Ceriani, M.F. (2021). Decapentaplegic Acutely Defines the Connectivity of Central Pacemaker Neurons in Drosophila. J Neurosci *41*, 8338-8350. 10.1523/JNEUROSCI.0397-21.2021.
99. Damulewicz, M., Doktor, B., Baster, Z., and Pyza, E. (2022). The Role of Glia Clocks in the Regulation of Sleep in Drosophila melanogaster. J Neurosci *42*, 6848-6860. 10.1523/JNEUROSCI.2340-21.2022.
100. Vaughen, J.P., Theisen, E., Rivas-Serna, I.M., Berger, A.B., Kalakuntla, P., Anreiter, I., Mazurak, V.C., Rodriguez, T.P., Mast, J.D., Hartl, T., et al. (2022). Glial control of sphingolipid levels sculpts diurnal remodeling in a circadian circuit. Neuron *110*, 3186-3205 e3187. 10.1016/j.neuron.2022.07.016.
101. Duhart, J.M., Herrero, A., de la Cruz, G., Ispizua, J.I., Pirez, N., and Ceriani, M.F. (2020). Circadian Structural Plasticity Drives Remodeling of E Cell Output. Curr Biol *30*, 5040-5048 e5045. 10.1016/j.cub.2020.09.057.

102. Gorostiza, E.A., Depetris-Chauvin, A., Frenkel, L., Pirez, N., and Ceriani, M.F. (2014). Circadian pacemaker neurons change synaptic contacts across the day. Curr Biol *24*, 2161-2167. 10.1016/j.cub.2014.07.063.
103. Fernandez, M.P., Pettibone, H.L., Bogart, J.T., Roell, C.J., Davey, C.E., Pranevicius, A., Huynh, K.V., Lennox, S.M., Kostadinov, B.S., and Shafer, O.T. (2020). Sites of Circadian Clock Neuron Plasticity Mediate Sensory Integration and Entrainment. Curr Biol *30*, 2225-2237 e2225. 10.1016/j.cub.2020.04.025.
104. Taniguchi, H., He, M., Wu, P., Kim, S., Paik, R., Sugino, K., Kvitsiani, D., Fu, Y., Lu, J., Lin, Y., et al. (2011). A resource of Cre driver lines for genetic targeting of GABAergic neurons in cerebral cortex. Neuron *71*, 995-1013. 10.1016/j.neuron.2011.07.026.
105. Madisen, L., Zwingman, T.A., Sunkin, S.M., Oh, S.W., Zariwala, H.A., Gu, H., Ng, L.L., Palmiter, R.D., Hawrylycz, M.J., Jones, A.R., et al. (2010). A robust and high-throughput Cre reporting and characterization system for the whole mouse brain. Nat Neurosci *13*, 133-140. 10.1038/nn.2467.
106. Byers, S.L., Wiles, M.V., Dunn, S.L., and Taft, R.A. (2012). Mouse estrous cycle identification tool and images. PLoS One *7*, e35538. 10.1371/journal.pone.0035538.
107. Susaki, E.A., Tainaka, K., Perrin, D., Kishino, F., Tawara, T., Watanabe, T.M., Yokoyama, C., Onoe, H., Eguchi, M., Yamaguchi, S., et al. (2014). Whole-brain imaging with single-cell resolution using chemical cocktails and computational analysis. Cell *157*, 726-739. 10.1016/j.cell.2014.03.042.
108. Bankhead, P., Loughrey, M.B., Fernandez, J.A., Dombrowski, Y., McArt, D.G., Dunne, P.D., McQuaid, S., Gray, R.T., Murray, L.J., Coleman, H.G., et al. (2017). QuPath: Open source software for digital pathology image analysis. Sci Rep *7*, 16878. 10.1038/s41598-017-17204-5.
109. Rocks, D., and Kundakovic, M. (2023). Hippocampus-based behavioral, structural, and molecular dynamics across the estrous cycle. J Neuroendocrinol *35*, e13216. 10.1111/jne.13216.
110. Woolley, C.S., Gould, E., Frankfurt, M., and McEwen, B.S. (1990). Naturally occurring fluctuation in dendritic spine density on adult hippocampal pyramidal neurons. J Neurosci *10*, 4035-4039. 10.1523/JNEUROSCI.10-12-04035.1990.
111. Woolley, C.S., and McEwen, B.S. (1992). Estradiol mediates fluctuation in hippocampal synapse density during the estrous cycle in the adult rat. J Neurosci *12*, 2549-2554. 10.1523/JNEUROSCI.12-07-02549.1992.
112. Christian, C.A., and Moenter, S.M. (2010). The neurobiology of preovulatory and estradiol-induced gonadotropin-releasing hormone surges. Endocr Rev *31*, 544-577. 10.1210/er.2009-0023.
113. Jacobs, G.H. (2013). Losses of functional opsin genes, short-wavelength cone photopigments, and color vision--a significant trend in the evolution of mammalian vision. Vis Neurosci *30*, 39-53. 10.1017/S0952523812000429.
114. Jacobs, G.H., Neitz, M., and Neitz, J. (1996). Mutations in S-cone pigment genes and the absence of colour vision in two species of nocturnal primate. Proc Biol Sci *263*, 705-710. 10.1098/rspb.1996.0105.
115. Baraas, R.C., Carroll, J., Gunther, K.L., Chung, M., Williams, D.R., Foster, D.H., and Neitz, M. (2007). Adaptive optics retinal imaging reveals S-cone dystrophy in tritan color-vision deficiency. JOSA A *24*, 1438-1447.
116. Kuchenbecker, J., Neitz, A., Rice, A., Casiraghi, L., Bussi, I., Buhr, E., Neitz, M., Neitz, J., and de la Iglesia, H. (2023). Toward an indoor lighting solution for social jet lag.
117. Cobb, J.K., Bialozynski, C., Neitz, J., Jacobs, G., and Neitz, M. (1999). UV cone pigment genes from Syrian and Siberian hamsters. In 4. (ASSOC RESEARCH VISION OPHTHALMOLOGY INC 9650 ROCKVILLE PIKE, BETHESDA, MD …), pp. S353-S353.
118. Williams, G.A., and Jacobs, G.H. (2008). Absence of functional short-wavelength sensitive cone pigments in hamsters (Mesocricetus). Journal of Comparative Physiology A *194*, 429-439.
119. Thompson, S., Recober, A., Vogel, T.W., Kuburas, A., Owens, J.A., Sheffield, V.C., Russo, A.F., and Stone, E.M. (2010). Light aversion in mice depends on nonimage-forming irradiance detection. Behav Neurosci *124*, 821-827. 10.1037/a0021568.
120. van der Vinne, V., Tachinardi, P., Riede, S.J., Akkerman, J., Scheepe, J., Daan, S., and Hut, R.A. (2019). Maximising survival by shifting the daily timing of activity. Ecol Lett *22*, 2097-2102. 10.1111/ele.13404.
121. Li, R., Miao, J., Fan, Z., Song, S., Kong, I.-k., Wang, Y., and Wang, Z. (2018). Production of genetically engineered golden Syrian hamsters by pronuclear injection of the CRISPR/Cas9 complex. JoVE (Journal of Visualized Experiments), e56263.
122. Neitz, M., Krekling, E.D., Hagen, L.A., Pedersen, H.R., Rowlan, J., Barborek, R., Neitz, J., Crain, A., and Baraas, R.C. (2020). Tritan color vision deficiency may be associated with an OPN1SW splicing defect and haploinsufficiency. JOSA A *37*, A26-A34.

VITA

2016-2018	Undergraduate Research Assistant, Gonzaga University, Advisor: Kylie Allen
2017	Summer Undergraduate Research Fellow, University of Washington, Advisor: Ramkumar Sabesan
Fall 2018 (rotation)	Graduate Student Research Assistant, University of Washington, Advisor: Horacio de la Iglesia
Winter 2019 (rotation)	Graduate Student Research Assistant, Fred Hutch Cancer Research Center, Advisor: Aakanksha Singhvi
Spring 2019 (rotation)	Graduate Student Research Assistant, Seattle Children's Research Institute, Advisor: Tim Cherry
2019-2023	Graduate Student Research Assistant, University of Washington, Thesis Advisor: Horacio de la Iglesia

Publications

Neitz, A., Jiang, X, Kuchenbecker J.A., Domdei, N., Harmening, Yan, H, Yeonan-Kim, Patterson, S.S., Neitz, M, Neitz, J., Coates, D., Sabesan, R. (2020) The effect of cone spectral topography on chromatic detection sensitivity. **J. Opt. Soc. Am. A Opt. Image Sci. Vis.** 37(4), A244-A254.

Tunçkanat, T., Gendron, A., Sadler, Z., **Neitz, A**., Byquist, S., Lie, T. J., & Allen, K. D. (2022) Lysine 2,3-aminomutase and a newly discovered glutamate 2,3-aminomutase produce β-amino acids involved in salt tolerance methanogenic archaea. Biochemistry 61(11), 1077-1090.

Bussi, I.L., **Neitz, A**., Sanchez, R.E.A., Casiraghi, L.P., Kunda, D., Allen, C.N., Evans, J.A., and de la Iglesia, H.O.. (2023) Expression of the vesicular GABA transporter within Neuromedin S+ neurons sustains behavioral circadian rhythms. **Proc. Natl. Acad. Sci. U.S.A.** *In Press*

Neitz A., Rice A, Casiraghi L, Bussi IL, Buhr ED, Neitz M, Neitz J, de la Iglesia HO, Kuchenbecker JA. Toward an indoor lighting solution for social jet lag. **Research Square**. 2023 Mar 17.

Neitz, A., Rice, A., Casiraghi, L., Bussi, I. L., Buhr, E.D., Neitz, M., Neitz, J. de la Iglesia, H. O. and Kuchenbecker, J. (***In Review***) Toward an indoor lighting solution for social jet lag.

Neitz, A., Carter, B., de la Iglesia, H.O. (in preparation) SCN-VIP neurons undergo a daily cycle of retraction and growth driven by the circadian clock.

Neitz, A., Neitz, M. & Neitz, J. (in preparation) Colorblindness confined to one eye

Abstracts

Neitz A., Jiang X, Patterson SS, Doebley A-L, Neitz M, Neitz J, Sabesan R. Color detection without hue perception. (2018) **Invest Ophthalmol Vis Sci.** 2018;59(9).

Neitz A., Doebley A-L, Patterson SS, Neitz M, Neitz J, Sabesan R. High acuity vision corrected for chromatic and monochromatic aberrations is associated with color discrimination without red-green or blue-yellow sensations. **Journal of Vision**. 2019

Patents

Patent Application 62/850,493 filed 5/20/2019
Materials and methods for controlling the activity of non-image forming visual pathways
Inventors: Jay Neitz, Maureen Neitz, James Kuchenbecker, Sara Patterson, **Alexandra Neitz**